

**Performance Investigation of  $H_\infty$   
Control and Port Controlled Hamilton  
with Dissipation Based Nonlinear  
Control for IPMSM Drives**

by

Zhuoqun Zhai

A thesis submitted in partial fulfillment of the requirement of the

M. Sc. degree in

Electrical and Computer Engineering department of

Lakehead University

Thunder Bay, Ontario

April 10, 2017

# Abstract

Within the field of electrical drive systems, there has been increasing popularity in the use of permanent magnetic synchronous machines as an execution unit, and the cooperation with high performance control strategy. Industrial engineers and researchers have developed countless applications with PM motors such as wind energy, hybrid vehicle and even in the elevator field. PMSM is a multivariate, nonlinear, time-varying system. Its entire operation is influenced by parameter variation, external load disturbance and unmodelled uncertainty. To eliminate such negative impacts and develop better performing PMSM control system, advanced control algorithms are critical.

Therefore, this thesis forces on developing two different control techniques such as mixed-sensitivity based  $H_\infty$  controller and port controlled Hamilton with dissipation (PCHD) controller to handle the uncertainties of the drives. Former one establishes the controller in terms of frequency domain, successfully converted IPMSM control problem to a standard  $H_\infty$  based mixed-sensitivity problem by selecting proper weight functions and solving its correspond Ricatti equations. While the latter one realizes the control objective in energy aspects by assigning interconnection and damping matrix for IPMSM system to prove its passivity and ensure global stability. The performances of both controllers for IPMSM drive have been investigated in both simulations and experiments using MATLAB-Simulink and dSPACE DSP board DS1104 for a 5 hp prototype motor. A direct current (DC) machine is coupled with IPMSM shaft to use as dynamic load. It is found that the performances of both controllers are robust at different operating conditions while PCHD exhibits better dynamic performance than that of  $H_\infty$  control.

## Acknowledgements

I would like to acknowledge my supervisor Dr. M. Nasir Uddin for his patience and guidance during my time at Lakehead University. His advising had encouraged me to successfully complete this program.

Appreciation are extended to Dr. Xiaoping Liu for his advising and availability throughout the Master's program. His suggestions are essential to the completion of this project.

I extend my thanks to members of the engineering department, who were involved in the thesis seminar and provided valuable feedback.

I appreciate my family and friends, as their mental support and contribution have always been indispensable to me.

Special thanks to Garin Schoonhoven and Mizanur Rahman for providing countless comments at all times even most of time they are not physically around. Also thanks to Ifta Amin who has always been by my side and had helped me to deal with academic obstacles.

Zhuoqun Zhai

# Contents

<b>1</b>	<b>Introduction</b>	<b>1</b>
1.1	Research Background . . . . .	1
1.2	Introduction of PMSM . . . . .	2
1.2.1	Motor Control Strategies: FOC . . . . .	4
1.3	Literature Review: Control Techniques . . . . .	6
1.3.1	Fixed Gain Control . . . . .	6
1.3.2	Model Based Control . . . . .	6
1.3.3	Intelligent Control . . . . .	10
1.4	IPMSM Drive System . . . . .	11
1.5	Thesis Overview and Organization . . . . .	12
<b>2</b>	<b>IPMSM Mathematical Modeling</b>	<b>14</b>
2.1	Introduction . . . . .	14
2.2	Coordinate Transformation . . . . .	15
2.3	System Modelling . . . . .	18
2.4	Conclusion . . . . .	23
<b>3</b>	<b><math>H_\infty</math> Controller for IPMSM Drive</b>	<b>24</b>
3.1	Introduction . . . . .	24
3.2	Preliminary Theory . . . . .	25

3.2.1	Riccati Equation and Hamiltonian Matrix . . . . .	25
3.2.2	$H_\infty$ norm . . . . .	25
3.2.3	IPMSM Modelling in Frequency Domain . . . . .	26
3.2.4	Standard $H_\infty$ Output Feedback Control . . . . .	28
3.3	$H_\infty$ controller with Mixed-sensitivity Approach . . . . .	31
3.4	Mixed-Sensitivity Based $H_\infty$ Controller for IPMSM . . . . .	33
3.4.1	Weight Function Selection and Controller Design . . . . .	35
3.5	Conclusion . . . . .	37
<b>4</b>	<b>Nonlinear PCHD Controller for IPMSM Drive</b>	<b>38</b>
4.1	Introduction . . . . .	38
4.2	Port Controlled Hamiltonian with Dissipation System . . . . .	40
4.3	PCHD Model for IPMSM . . . . .	46
4.4	Load Torque Observer Design . . . . .	50
4.5	Conclusion . . . . .	52
<b>5</b>	<b>System Simulation</b>	<b>54</b>
5.1	Introduction . . . . .	54
5.2	Simulation Results . . . . .	56
5.2.1	Simulation Results of $H_\infty$ Controller . . . . .	56
5.2.2	Simulation Results of PCHD Controller . . . . .	63
5.3	Conclusion . . . . .	67
<b>6</b>	<b>Real Time Implementation</b>	<b>68</b>
6.1	Hardware Overview . . . . .	68
6.2	Experimental Results . . . . .	72
6.3	Conclusion . . . . .	78

<b>7 Conclusion</b>	<b>79</b>
7.1 Achievements . . . . .	79
7.2 Future scope of the work . . . . .	80
<b>A IPMSM Parameters</b>	<b>90</b>
<b>B Simulation Code and Schematic</b>	<b>91</b>
B.1 $H_\infty$ controller offline tuning code . . . . .	91
B.2 Simulation and Real-time Schematic . . . . .	92
B.2.1 Simulation Schematic . . . . .	92
B.2.2 PCHD Controller Schematic . . . . .	96
B.3 Real-time Schematic . . . . .	97

# List of Figures

1.1	Surface mounted magnets motor. . . . .	3
1.2	Surface inserted magnets motor. . . . .	3
1.3	Radial interior magnets motor. . . . .	3
1.4	Axial interior magnets motor. . . . .	3
1.5	Motor rotation principle . . . . .	4
1.6	One set of magnets . . . . .	4
1.7	Magnetic flux in d-q axis . . . . .	5
1.8	Typical three phase driving system. . . . .	12
2.1	Reference frame conversion . . . . .	15
2.2	All reference frame vectors . . . . .	17
2.3	Motor d-axis equivalent circuit . . . . .	21
2.4	Motor q-axis equivalent circuit . . . . .	21
2.5	General IPMSM phasor diagram. . . . .	22
2.6	Phase diagram with $i_d \equiv 0$ scenario. . . . .	22
3.1	Block diagram of $H_\infty$ based IPMSM. . . . .	26
3.2	Simplified Block diagram of Fig. 3.1. . . . .	27
3.3	Standard $H_\infty$ control system. . . . .	28
3.4	A basic feedback control system. . . . .	31

3.5	Block diagram of $H_\infty$ mixed sensitivity . . . . .	33
3.6	Block diagram for every sensitivity function . . . . .	34
5.1	IPMSM speed control system schematic in Simulink software. . .	55
5.2	Frequency characteristics of sensitivity function and complementary sensitivity function: (a)sensitivity function (b)complementary sensitivity function . . . . .	57
5.3	Responses of the proposed $H_\infty$ controller for a ramp speed reference signal: (a) speed response overview (b) zoom in view from 0.5 to 1 s (c) d-q axis currents response (d) d-q axis currents response of PI controller (e) speed error comparison (f) single phase current of $H_\infty$ controller. . . . .	59
5.4	Response of the proposed $H_\infty$ controller for step changes speed reference signal from 100 – 160 – 120 rad/s (a) speed response overview (b) zoom in view from 1.5 to 2 s (c) d-q axis currents response of $H_\infty$ controller (d) d-q axis currents response of PI controller (e) speed error comparison (f) single phase current of $H_\infty$ controller . . . . .	60
5.5	Performance of the proposed $H_\infty$ based IPMSM drive for ramp changes in external load: (a) comparative speed responses (b) speed error comparison (c) d-q axis currents response of $H_\infty$ controller (d) d-q axis currents response of PI controller . . . . .	62
5.6	Performance of the proposed $H_\infty$ controller with parameter variations.	63
5.7	Balanced three phased currents for $H_\infty$ controller. . . . .	63

5.8	Response of the proposed nonlinear PCHD controller for a ramp reference signal: (a) speed response overview (b) speed error comparison with conventional tuned PI controller (c) d-q axis currents response (d) single phase current of PCHD controller. . . . .	64
5.9	Response of the proposed nonlinear PCHD controller for step changes reference speed signal: (a) speed response overview (b) speed error comparison (c) d-q axis currents response (d) single phase current response. . . . .	65
5.10	Performance of the proposed nonlinear PCHD controller based IPMSM drive for ramp changes in external load: (a) comparative speed response (b) speed error dynamic comparison (c) d-q axis currents response(d) single phase current response . . . . .	66
5.11	Error dynamics of proposed torque observer (a) ramp speed reference signal (b) step speed reference signal (c) external load variation signal	67
6.1	Block diagram of real-time hardware setup of experimental system based on DS1104 board. . . . .	69
6.2	Experimental setup environment for the complete IPMSM drive. .	70
6.3	CP1104 connection panel . . . . .	71
6.4	Experimental starting performance of the IPMSM drive: (a) speed response for conventional tuned PI controller (b) d-q axis current response for conventional tuned PI controller (c) speed response for proposed $H_\infty$ controller with mixed-sensitivity approach (d) d-q axis current response for proposed $H_\infty$ controller (e) speed response for proposed nonlinear PCHD controller (f)d-q axis current response for proposed nonlinear PCHD controller. . . . .	74

6.5	Experimental performance of IPMSM drive with various controller for step changes in command speed 30-100rad/s with 25% rated load (a) speed response for conventional tuned PI controller (b) d-q axis current response for conventional tuned PI controller (c) speed response for $H_\infty$ controller (d) d-q axis current response for $H_\infty$ controller (e) speed response for nonlinear PCHD controller (f) d-q axis current response nonlinear PCHD controller. . . . .	75
6.6	Experimental performance of IPMSM drive with various controller for steady command speed in 70rad/s with 50% rated load (a) speed response for conventional tuned PI controller (b) d-q axis current response for conventional tuned PI controller (c) speed response for $H_\infty$ controller (d) d-q axis current response for $H_\infty$ controller (e) speed response for nonlinear PCHD controller (f) d-q axis current response nonlinear PCHD controller. . . . .	76
6.7	Experimental performance for balanced three phase currents: (a) $H_\infty$ controller (b) nonlinear PCHD controller . . . . .	77
B.1	Sybsystem of PWM generation . . . . .	92
B.2	Subsystem of d-q axis voltage to a-b-c axis voltage . . . . .	93
B.3	Subsystem of d-q axis current to a-b-c axis current . . . . .	93
B.4	Subsystem of inverter . . . . .	93
B.5	Subsystem of $\alpha$ - $\beta$ axis voltage to d-q axis voltage . . . . .	94
B.6	Subsystem of rotor speed . . . . .	94
B.7	Subsystem of rotor current . . . . .	95
B.8	PCHD controller Simulink Blocks. . . . .	96
B.9	Real-time Simulink Blocks. . . . .	97

# List of Symbols

Symbol	Explanation
$U_s$	stator voltage
$i_d, i_q$	d-q axis current in rotating reference frame
$L_d, L_q$	d-q axis inductance
$\omega_r$	angular shaft velocity
$\delta$	power angel
$\cos\psi$	power factor
$R_s$	stator resistance
$\phi_m$	rotor magnetic flux
$\phi_d, \phi_q$	d-q axis magnetic flux
$N_p$	motor pole of pair
$\tau_e$	electromagnetic torque
$\tau_L$	external load of torque
$J$	inertia constant
$B_m$	damping coefficient
$G(s)$	transfer function of argument plant
$P(s)$	transfer function of nominal plant
$C(s)$	transfer function of proposed controller
$S(s)$	transfer function of sensitivity
$T(s)$	transfer function of complementary sensitivity
$\Delta(s)$	perturbation model
$W_1, W_2, W_3$	weight function
$H(x)$	Hamiltonian function

Symbol	Explanation
$J(x)$	interconnection matrix
$J_{12}, J_{13}, J_{23}$	design coefficients of interconnection matrix
$R(x)$	damping function
$r_1, r_2, r_3$	design coefficients of damping matrix
$\hat{\omega}_r, \hat{\tau}_L$	observed motor shaft velocity and observed external load of torque
$k_1, k_2$	design coefficients of load observer
$\omega_r^*, \tau_L^*$	command motor shaft velocity and command external load of torque

# Chapter 1

## Introduction

### 1.1 Research Background

A world without any motor is difficult to imagine. Electric motors consume more than half of total electrical energy produced in the world. From the smallest motor found in a quartz watch to the largest unit capacity of 800 megawatts motor that is used in a hydro power station in China [1], motors are implemented in many diverse applications. The first electric motor born in 1850s was the permanent magnet motor. Since the permanent magnet material could not meet the power requirement of industry for a long time, excitation motors predominate the mainstream. AlNiCo invented by Bell Lab during 1930s and Ferrite discovered in 1950s pressed the acceleration pedal for permanent magnet (PM) motors. Although limitations like low coercivity had result in low remanence density reducing magnetic field. Things changed tremendously when Neodymium magnet was introduced into the field, especially in the fields of aerospace, CNC machine, robot, etc.

PM motor with Neodymium magnet inside allows it to become a representative

of high power density and high efficiency motors. PM motors' advantages such as simple structures, flexible control algorithm, multiple rotor forms makes it better for optimal control design, inevitably replacing traditional AC induction motors in some precise application scenarios. Drawbacks are the high cost of the machine itself and its complex control as it is heavily influenced by parameters variation, unstructured uncertainty and nonlinearity. Thus, the main objective of this thesis is to develop relatively robust control algorithms.

## 1.2 Introduction of PMSM

As a mechanical-electrical conversion equipment, motors achieves mutual exchange between mechanical energy and electrical energy via magnetic field in the air gap. According to the Least Action Principle, most of magnetic energy are stored in the air gap. During the convention process, magnetic energy will not be consumed. This type of media could be excited by current in windings or generated by permanent magnets. In order to maintain the current, non-superconductive windings need to consume energy constantly. However, permanent magnets could establish a continuous magnetic field without energy injection. Therefore, motors built by PM materials has simpler structures and lower energy consumption. This section will introduce the basic idea about Permanent Magnet Synchronous Motor (PMSM).

PM motors are varied by sinusoidal wave PM motors and square wave PM motors, and the latter one is also called brushless DC motors. This thesis is based on sinusoidal wave PM motors. Sinusoidal wave PM motors are classified by how magnets were placed in the rotor. Fig.(1.1) to Fig.(1.4) illustrate four ways to place

magnets such as, surface-mounted, surface-insert, interior-radial and interior-axial respectively.

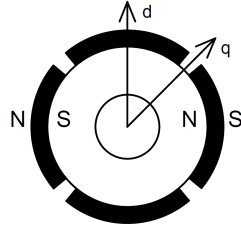


**Figure 1.1:** Surface mounted magnets motor.

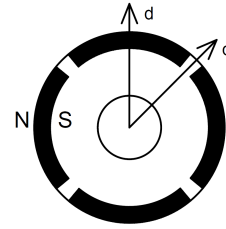


**Figure 1.2:** Surface inserted magnets motor.

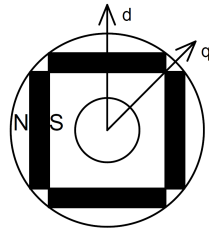


**Figure 1.3:** Radial interior magnets motor.

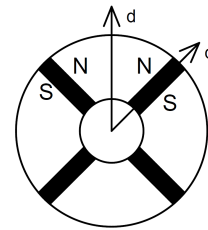


**Figure 1.4:** Axial interior magnets motor.

Due to magnetic flux generated by permanent magnet directly goes to air gap and doesn't go through any media like iron, surface-mounted PM motors have a symmetrical rotor magnetic circuit, evenly air gap and direct axis inductance is equal to quadrature axis inductance. This type of arrangement usually lack of mechanical robustness due to magnets are not snugly fitted into rotor lamination. Thus, this motor is not suitable for high speed application. Magnets were completely buried into the rotor lamination in surface-inserted PMSM has better mechanical strength. However, gaps exist between the magnets and the rotor lamination weaken structural strength more or less.

Interior type PM motors in Fig.1.3 and Fig.1.4 provide the greatest mechanical structure. Therefore, suited for high-speed applications. It doesn't have symmetrical rotor magnetic circuit and even air gap, direct inductance is smaller than quadrature inductance. Axial type interior PMSM requires a large volume of PMs, making this configuration not suitable for widely application since they are expen-

sive. Radial type and interior type PM motors have larger salient rate, providing higher power density, better overload abilities and easier for flux weakening control. Therefore, this thesis considers radial arrangement PM motors as research target.

### 1.2.1 Motor Control Strategies: FOC

Every AC motor is driven by a rotating magnetic field as shown in Fig.1.5 which is generated by symmetry current. Noted that both inside and outside circle could be defined as stator or rotor based on the designer's will. In this thesis, the outside loop is considered as stator and the inside loop is considered as rotor. For PM motors, magnets on the stator are equivalent to the stator currents, while rotor magnets are the real magnet.

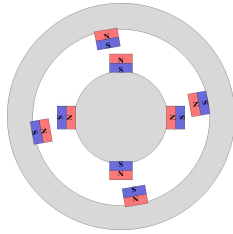


Figure 1.5: Motor rotation principle

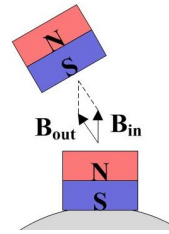
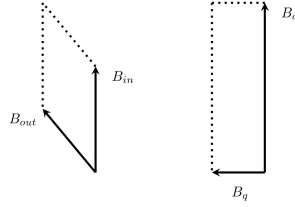


Figure 1.6: One set of magnets

The air gap between magnets and the shaft are fixed, making the torque is related to the magnetic force between stators and rotors. Which derives a solid conclusion: the torque is directly bounded with the magnetic flux density and the position of magnets. Fig.1.6 focus on one set of magnets.  $B_{in}$  is the lower magnetic flux while  $B_{out}$  represents the upper one. The area of the parallelogram surrounded by them is proportional to the torque. If  $B_{in}$  and  $B_{out}$  is projected to a Cartesian coordinate system in Fig.1.7, magnetic flux on direct axis and quadrature axis (shown as  $B_d$  and  $B_q$  respectively) could be easily derived.



**Figure 1.7:** Magnetic flux in d-q axis

When the inductance of three phase motor is converted to “ $d - q$ ” axis components, the magnetic flux can be calculated. So that torque can be found when calculating magnetic force. Based on torque, the speed or position can be controlled easily. That is the basic idea of vector control, also known as Field Oriented Control (FOC) which was invented by K. Hasse [2] and F. Blaschke [3] in 1970s. FOC provides a way to uncouple torque and magnetic flux. Meanwhile, motor performance could be reached by much more efficient strategies such as constant torque angle control, unity power factor control, constant mutual air gap flux-linkages control, maximum torque per ampere control (MPTA) and minimum loss or maximum efficiency control, etc.

(1) Constant torque angle control

Constant torque angle control meaning torque angle is maintained at 90 degree. Thus current generated by flux (direct-axis current) is zero, avoiding demagnetization effect and leaving torque current (quadrature-axis current) exists only. This mode operates under the rated speed and commonly used in many motor drive system. However, the drawback is that motor terminal voltage will increase when apply heavy load, requiring larger inverter capacity.

(2) Maximum torque per ampere control

In MTPA algorithm, PMSM stator current remains minimum value under

desired torque. MTPA provides lowest current with the same torque, eliminating copper loss and promoting efficiency.

Vector control have advantages such as good torque response, accurate speed control and full torque at zero speed. However, vector control depends on the complex Park-Clark coordinate transformations, heavy computation and accurate mathematical model. Thus, it reduces the control performance.

## 1.3 Literature Review: Control Techniques

### 1.3.1 Fixed Gain Control

PID control favoured in industries due to simplicity and easy implementation. However, because of the limitation such as excessively tuning parameters, experiences required in parameters tuning, and parameters highly coupled, pushing researchers to look for other control techniques. In [4], authors combined PID with fuzzy logic control by switching control strategy to reach better performance. In [5] authors tuned PID parameters using fuzzy control. In addition, [6] application was reported mixing neuro-network and PID controller.

### 1.3.2 Model Based Control

With improving performance and decreasing cost of microprocessor, many advanced control algorithms are implemented into PMSM drive systems. Some off them are discussed below.

- (1) Adaptive Control

Adaptive control technology can modify control programs and parameters based on certain mathematical models and algorithms in order to improve control performance when operating condition changes. Adaptive control method estimates uncertain objectives and changes control gains online based on measured signal. Method like fuzzy-adaptive control [7], adaptive parameters identification [8,9], model reference adaptive control [10–12] and nonlinear adaptive control are commonly used. In principle, it can be applied to any dynamic structure uncertain models or parameter uncertain models. However, this method requires processors to offer complex computation capability.

### (2) Back-stepping Control

As a relatively newly developed control strategy proposed in 1991 [13, 14], back-stepping method designs controllers by adjusting its algorithm step by step to reach globally stable and tracking ability. At every step, the control makes virtual error converge to zero until real control elements appeared. Intrinsically, it is a stationary compensation concept, the former subsystems stabilized by virtual control of the latter subsystem. However, the backstepping method also requires complex computations. [15, 16]

### (3) Sliding Model Control

Sliding model control (SMC) uses switch control algorithm keeping system response tracking desired path dealing with parameters change and load variations. It shows a discontinued control characteristic [17, 18]. According to errors and its derivative SMC constrain the system to operate on the desired track. Besides, SMC doesn't require model identification, making it easy to implement. However, system could have chattering effect due to its switching features. This mainly hap-

pens as the acceleration ability is constrained by objective factors. The existence of system inertance, switching time lagging lead to “quasi sliding mode”. In AC servo drive systems, SMC preforms a unique advantage as anti-interference ability. In [19], author introduced SMC into direct torque controlled PM motors, replacing hysteresis controllers by torque and flux, maintaining inverter switching frequency stable. In [20] author analyzed the reason behind chattering and proposed a optimization plan.

#### (4) Robust $H_\infty$ Control

Canadian researcher George Zames introduced  $H_\infty$  into control theory for the first time in 1981 [21]. His article used  $H_\infty$  norm as optimize indexes for transfer functions of control system. Dolye presented structure singularity to solve robust performance problems when structure uncertainty exists in controlled model in 1982 [22]. Based on that,  $\mu$  theory had been emerged. Francis and Zames introduced preliminary solution of  $H_\infty$  in the next year based on Nevanlinna-Pick interpolation. And Dolye et.al enriched it to MIMO systems [23]. Following researchers called this phase as “Classic  $H_\infty$  Theory”. Dolye and his collages proved two appropriate Ricatti equations could solve  $H_\infty$  problem, its order equal to the order of controlled system [24]. Then he proposed a method to find  $H_\infty$ 's solution within one Ricatti equation. This theory was going down in history as a milestone indicating  $H_\infty$  control had moved to maturity. In 1989,  $H_2/H_\infty$  control was introduced by Bemstein et.al [25]. They combined the advantages of  $H_2$  and  $H_\infty$  reaching faster adjustment ability and remain robustness. Farlane invented a procedure of loop-shaping method in 1992 [26].

Many studies related to  $H_\infty$  were reported. And  $H_\infty$  theory was not only used in engineering field but also used to solve the problem in economics. Even so, there

are several problems waiting to be solved, including weight functions' selection. For a long time, different objectives need unique weight functions. Selection of weight functions fully depends on designer's experiences. Besides,  $H_\infty$  controllers usually equipped in high order and hardly to be implemented in real-time field.

Implementing  $H_\infty$  algorithm especially mixed-sensitivity on permanent magnet synchronous motor could be traced back to 10 years ago. Yinhua Chang firstly implement  $H_\infty$  controller in a micro-PMSM motors, but still lacking of application in large machinery [27]. Guorong Wu et.al set  $H_\infty$  controller in q-axis loop in order to achieve speed tracking performance and a PI controller is used for d-axis loop [28]. Overall, mixed-sensitivity control approach is still a PID like linear controller. Hence, this controller is not suitable for AC motor drive. Therefore, researchers utilized the following nonlinear approach.

#### (5) Passive Control

Hamilton system widely exists in physical, biological and engineering field. Many of mechanics model are presented in the form of Hamilton system. In a large amount of controller design, energy concept applied on an immense scale [29–33]. Physical explanation of control activity could be explained from energy prospective, so that designing controller from energy side is both physically and geometrically significant. Ortega summarized Hamilton system theory to a complete non-linear control theory [34].

Energy shaping was driven notable results [35, 36] in early stage. Ortega et.al were inspired and introduced Passivity Based Control (PBC) successfully for AC motor control [34, 37–39]. Passivity represent the following characteristic: if the total energy of a system always small or equal to the summation of initial energy and energy obtained outside at any time, the system is passive system. Passivity

theory can be applied to AC motor control by analyzing Euler-Lagrange equation of motors, representing motors with two passive sub-systems in series. Again, with the help of the relation between passivity and stability, the system global stability can be guaranteed from energy shaping side. Most commonly used methods are controlled Lagrangian [40–42] and Interconnections and Damping Assignment and Passivity-based Control (IDA-PBC) [43–45]. Applications of IDA-PBC are full bridge rectifier [46], pendulum [47], robot arm [48], energy management and storage system [49], spacecraft [50], etc. Dissipation theory was introduced into Port-Controlled Hamiltonian System (PCH) and turned into Port-Controlled Hamiltonian with Dissipation (PCHD), which applied in IDA-PBC to represent the system. Energy conservation could be achieved by proper interconnection and damping assignment to keep the system import the same amount of energy as export maintaining energy homeostasis.

For PCHD represented nonlinear system, stabilization controller for equilibrium point was designing by assign interconnection and damping equations. Preliminary attempts [45] established mathematical model of PM motor in PCHD structure, designed load observer targeting unknown load torque. PCHD principle can be summarized as: for a specified PCHD system and its desired equilibrium point, find a feedback stabilization control to stabilize the system at set point. Or, minimize the energy function at equilibrium point by feedback loop. In [51], authors proved and discussed PCHD feedback in general.

### 1.3.3 Intelligent Control

Intelligent control is emerging in automatic control, eliminating problems that classical control theory could not handle. Intelligent controllers design does not depend on mathematical model of the system. By inheriting non-linearity of

human brain, intelligent control overcomes system uncertainties and non-linearity, enhancing system robustness. Major types of intelligent control are expert control, fuzzy logic control, neural network control, etc. Although it comes to fruition with each passing day, lacking foresight of objectivity, requiring complex computation that restrict its development.

Fuzzy logic control consists of fuzzifier, fuzzy interface engine and defuzzifier. It can closely imitate skilled operator and expert's control experience. Fuzzy logic control usually combined with other algorithms to reach better performance, such as fuzzy PID [52–54], adaptive fuzzy [55, 56], neruo-fuzzy, etc.

Neural network control (NNC) technique was proposed by neurophysiologist Warren McCulloch and mathematician Walter Pitts in 1943 based on electrical circuit formed neural network model [57]. In certain degree, neural-network imitate human thought, such as distribute information storage and parallel process. Massive neurons formed network could make abundant activities. This idea was also applied in AC motor drives system. [58, 59] replace classical PID control for speed and position regulation. In [60] authors applied neural-network for online parameter identification. In [61, 62] authors utilized NNC to estimate rotor magnetic flux accurately that to achieve sensorless control.

Although neural-network has numerous achievements, limitations like complex structure, tedious algorithm, lacking theoretical support for the selection of amount of hidden layer and neurons restrain its wide applications in industry.

## 1.4 IPMSM Drive System

Figure 1.8 illustrate the typical FOC controlled motor drive system. Almost every AC motor drive systems can use this set up after a little modification. It is a

duo feedback loop control schematic in general (current loop and speed loop), and comprised by several major component blocks: a three-phase two-level six switches IGBT inverter operated by pulse width modulation (PWM) signal. Speed sensor measure the motor position and then it is feedback to the controller. Algorithm is pre-installed in the controller to calculate command voltage based on sensors' signal. Coordinate transformation translate command voltage into sine-triangle based PWM signal in order to switch IGBTs correctly. Each blocks are specified in relative section of this thesis including equation derivations.

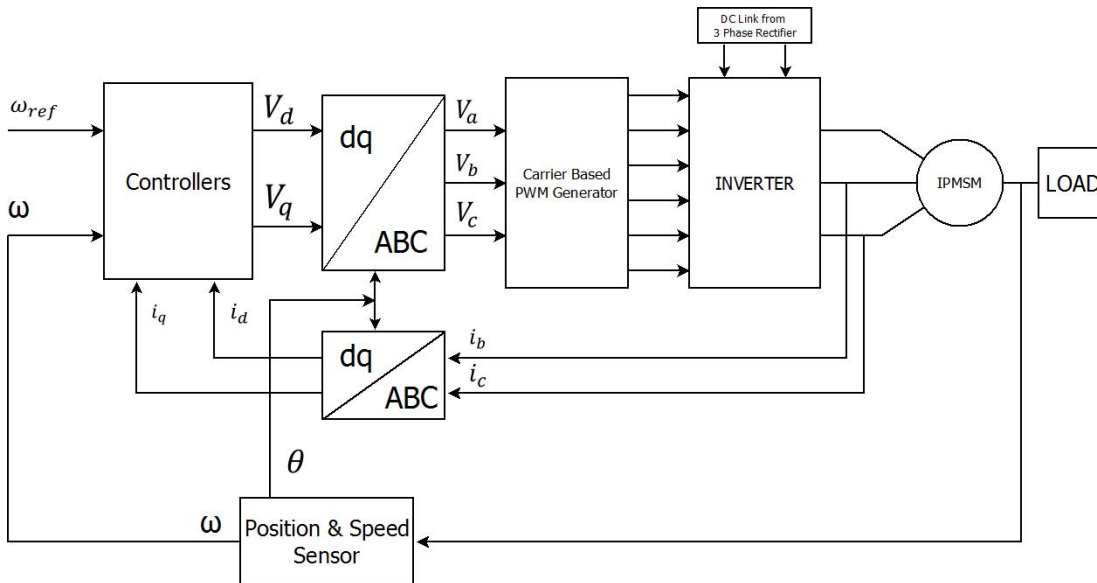


Figure 1.8: Typical three phase driving system.

## 1.5 Thesis Overview and Organization

This thesis is arranged according to research procedures. Each chapter covers a specific area related to the topic including illustration equations, tables, graphics and charts. The overview of each section are listed as follows.

Chapter 1 contains a brief introduction of the history about motor drive systems especially PM motor drive. This section also shows the comparison of different

types of PM motors along with their uniqueness. In addition, this part also provided the literature review on control techniques.

Chapter 2 derives the mathematical model of PMSM in detail, including coordinate transformation and IPMSM equivalent circuits in rotation frame.

From frequency domain, chapter 3 approves the stability of  $H_\infty$  robust controller utilizing mixed-sensitivity approach and detailed the procedure in how to find proper controller.

In terms of energy, chapter 4 provides a method to design a PCHD (port-controlled Hamilton system with dissipation) controller.

Chapter 5 bases on the controllers designed in previous two chapters, showing results from each algorithm in Matlab simulation environment. Examining the feasibility by load varying on different parameters and target speeds before moving to the real-time environment experiment.

Chapter 6 explain the real-time implementation procedure for the complete drive system on DSP board DS1104.

Final chapter 8 summarizes the thesis results and provide the possible optimization solution. It also includes potential future works.

# Chapter 2

## IPMSM Mathematical Modeling

### 2.1 Introduction

The process of deriving mathematical model of IPMSM is detailed in this section. It begins with conveying stator equations in a three stationary frame. Coordinate transformation named “Clark-Park transformation” provide the possibility to simplify the complex nonlinear expression.

Mathematical model of IPMSM could be developed by a two-phase motor which their winding located in “direct” and “quadrature” axis. The reason why implementing this method due to easy-to-understand theory. The stator only obtained one set of two windings while the rotor has only magnets. To be noticed is that d-axis is chosen to be parallel to the direction of magnetic flux. As a convention of Institute of Electrical and Electronics Engineers (IEEE), q-axis is defined by legging d-axis 90 electrical degree. These labels are used throughout this thesis sustainedly.

## 2.2 Coordinate Transformation

In order to reduce complexity of calculations, all the equations have to be transformed to synchronously rotating rotor reference frame where the machine equations are no longer rely on rotor position. Coordinate transformation has infinite solutions without certain limitations. Power equivalency is applied during the convention to maintain the uniqueness of transformation. The conversion process from stationary “A-B-C” frame to rotating “d-q-0” frame is divided into two steps, as shown in Fig.2.1. Firstly, stationary “A-B-C” frame is translated into stationary “ $\alpha - \beta - 0$ ” frame, which is known as Clark’s transformation and then from stationary “ $\alpha - \beta - 0$ ” frame to rotating “d-q-0” frame, which is known as Park’s transformation. Also, Fig.2.2 shows the relative positions of all the coordinate systems.

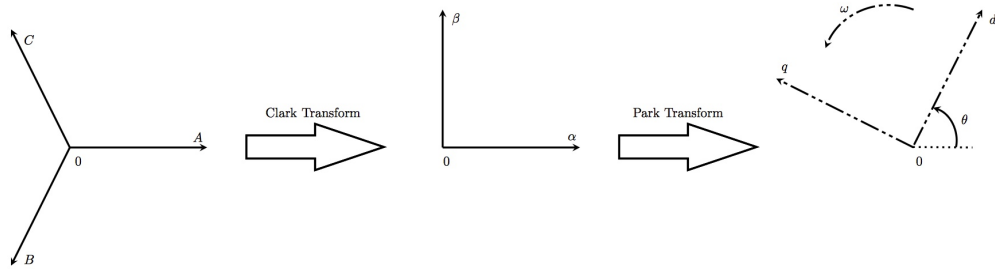


**Figure 2.1:** Reference frame conversion

Clark transformation can be labelled as 3s/2s transformation defined  $\alpha$ -axis coincides with A-axis and  $\beta$ -axis leading alpha axis a  $90^\circ$  electrical. The following vectors are defined as follows.

$$N_2 \cdot i_\alpha = N_3 \cdot i_A - N_3 \cdot i_B \cdot \cos 60^\circ - N_3 \cdot i_C \cdot \cos 60^\circ = N_3 (i_A - 0.5i_B - 0.5i_C)$$

$$N_2 \cdot i_\beta = N_3 \cdot i_B \cdot \sin 60^\circ - N_3 \cdot i_C \cdot \sin 60^\circ = \frac{\sqrt{3}}{2} N_3 (i_B - i_C)$$

$$N_2 \cdot i_0 = C_0 \cdot N_3 \cdot (i_A + i_B + i_C)$$

(2.1)

Where  $N_2$  and  $N_3$  are the proportionally constant that maintains power equivalency between the reference frames. For balanced system, 0-axis component becomes zero.

Rewrite (2.1) in the form of matrix,

$$\begin{bmatrix} i_\alpha \\ i_\beta \\ i_0 \end{bmatrix} = \frac{N_3}{N_2} \cdot \begin{bmatrix} 1 & -0.5 & -0.5 \\ 0 & \frac{\sqrt{3}}{2} & -\frac{\sqrt{3}}{2} \\ C_0 & C_0 & C_0 \end{bmatrix} \cdot \begin{bmatrix} i_A \\ i_B \\ i_C \end{bmatrix} = T_{3s/2s} \cdot \begin{bmatrix} i_A \\ i_B \\ i_C \end{bmatrix} \quad (2.2)$$

In order to determine  $N_3$ ,  $N_2$  and  $C_0$ , a characteristic of square matrices is used that is  $T_{3s/2s} \cdot T_{3s/2s}^{-1} = I$ .

$$\frac{N_3^2}{N_2^2} \cdot \begin{bmatrix} 1 & 0 & C_0 \\ -0.5 & \frac{\sqrt{3}}{2} & C_0 \\ -0.5 & \frac{\sqrt{3}}{2} & C_0 \end{bmatrix} \cdot \begin{bmatrix} 1 & -0.5 & -0.5 \\ 0 & \frac{\sqrt{3}}{2} & \frac{\sqrt{3}}{2} \\ C_0 & C_0 & C_0 \end{bmatrix} = \begin{bmatrix} 1 & 0 & 0 \\ 0 & 1 & 0 \\ 0 & 0 & 1 \end{bmatrix} \quad (2.3)$$

Thus, from Equ.(2.3), the following relationships could be extracted

$$\begin{aligned} \frac{N_3^2}{N_2^2} + \frac{N_3^2}{N_2^2} \cdot C_0^2 &= 1 \\ -\frac{1}{2} \cdot \frac{N_3^2}{N_2^2} + \frac{N_3^2}{N_2^2} \cdot C_0^2 &= 0 \end{aligned}$$

Therefore,  $\frac{N_3}{N_2}$  and  $C_0$  can be solved as:  $\frac{N_3}{N_2} = \sqrt{\frac{2}{3}}$ ,  $C_0 = \frac{1}{\sqrt{2}}$ .

Thus, the power invariant Clark's transformation can be illustrated as:

$$T_{3s/2s} = \sqrt{\frac{2}{3}} \cdot \begin{bmatrix} 1 & -0.5 & -0.5 \\ 0 & \frac{\sqrt{3}}{2} & -\frac{\sqrt{3}}{2} \\ \frac{\sqrt{2}}{2} & \frac{\sqrt{2}}{2} & \frac{\sqrt{2}}{2} \end{bmatrix} \quad (2.4)$$

Following equation represents the corresponding inverse transformation of (2.4).

$$T_{2s/3s} = \begin{bmatrix} \frac{2}{3} & 0 & \frac{\sqrt{2}}{3} \\ -\frac{1}{3} & \frac{\sqrt{3}}{3} & \frac{\sqrt{2}}{3} \\ -\frac{1}{3} & -\frac{\sqrt{3}}{3} & \frac{\sqrt{2}}{3} \end{bmatrix} \quad (2.5)$$

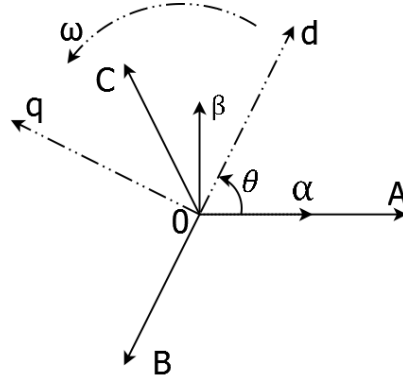


**Figure 2.2:** All reference frame vectors

Before applying the Park's transformation, the relation between rotational angle  $\theta$  and angular velocity is employed as follows

$$\theta = \int_0^t \omega(t) dt + \theta_0 \quad (2.6)$$

Where  $\theta_0$  is the initial angle difference between A-axis and q-axis.

Park transformation or 2s/2r transformation choose d axis align with the rotor magnetic flux and lagging q axis 90 electrical degrees. “d-q-0” reference frame is rotating as the angular velocity of  $\omega$ . With the help of Fig.(2.2), stationary “ $\alpha - \beta$ ” reference frame could be converted to synchronously “d - q” reference frame as:

$$\begin{aligned} i_d &= i_\alpha \cdot \cos(-\theta) + i_\beta \cdot \cos(\theta - 90^\circ) = i_\alpha \cdot \cos(\theta) + i_\beta \cdot \sin(\theta) \\ i_q &= -i_\alpha \cdot \sin(\theta) - i_\beta \cdot \sin(\theta - 90^\circ) = i_\alpha \cdot [-\sin(\theta)] + i_\beta \cdot \cos(\theta) \end{aligned} \quad (2.7)$$

From the above equations, Park's transformation matrix can be written as:

$$T_{2s/2r} = \begin{bmatrix} \cos \theta & \sin \theta \\ -\sin \theta & \cos \theta \end{bmatrix} \quad (2.8)$$

The inverse of Park's transformation can be defined as

$$T_{2r/2s} = \begin{bmatrix} \cos \theta & -\sin \theta \\ \sin \theta & \cos \theta \end{bmatrix} \quad (2.9)$$

By combining Clark's and Park's transformation equations (2.4) and (2.8), or their inverse equations (2.5) and (2.9), an direct relation between the three phase stationary frame and rotating frame can be explained by the following equations.

$$T_{3s/2r} = \begin{bmatrix} \sin \theta & \cos \theta & 1 \\ \sin(\theta - 120^\circ) & \cos(\theta - 120^\circ) & 1 \\ \sin(\theta + 120^\circ) & \cos(\theta + 120^\circ) & 1 \end{bmatrix} \quad (2.10)$$

$$T_{2r/3s} = \frac{2}{3} \cdot \begin{bmatrix} \sin \theta & \sin(\theta - 120^\circ) & \sin(\theta + 120^\circ) \\ \cos \theta & \cos(\theta - 120^\circ) & \cos(\theta + 120^\circ) \\ 0.5 & 0.5 & 0.5 \end{bmatrix} \quad (2.11)$$

## 2.3 System Modelling

The following assumptions are made for the motor to develop its dynamic model:

1. Each stator winding is separated from the other 120°.
2. The inductance is not affected by the current and varying with the rotor position sinusoidally.

3. The electrical conductivity of permanent magnet material is treated as zero.
4. Eddy currents and hysteresis loss are neglected.

The stator flux of PMSM is generated by three-phase current in the stator and permanent magnets in the rotor. Both stator flux and rotor flux are related to rotor position. Hence, for any Wye and Delta connected motor, a three phase mathematical model can be written as follows.

$$\begin{bmatrix} u_a \\ u_b \\ u_c \end{bmatrix} = R_s \times \begin{bmatrix} i_a \\ i_b \\ i_c \end{bmatrix} + \frac{d}{dt} \times \begin{bmatrix} \phi_a \\ \phi_b \\ \phi_c \end{bmatrix} \quad (2.12)$$

where,  $u_a, u_b, u_c$  are the stator voltage for each phase;

$i_a, i_b, i_c$  are the stator current for each phase;

$\phi_a, \phi_b, \phi_c$  are the magnetic flux for each phase.

The corresponding magnetic fluxes in the stator is defined as follows.

$$\begin{bmatrix} \phi_a \\ \phi_b \\ \phi_c \end{bmatrix} = \begin{bmatrix} L_{aa} & L_{ab} & L_{ac} \\ L_{ab} & L_{bb} & L_{bc} \\ L_{ac} & L_{bc} & L_{cc} \end{bmatrix} \times \begin{bmatrix} i_a \\ i_b \\ i_c \end{bmatrix} + \begin{bmatrix} \phi_{pa} \\ \phi_{pb} \\ \phi_{pc} \end{bmatrix} \quad (2.13)$$

where,  $L_{aa}, L_{bb}, L_{cc}$  are the self inductance for each phase;

$L_{ab}, L_{ac}, L_{bc}$  are the mutual inductance for each phase;

$\phi_{pa}, \phi_{pb}, \phi_{pc}$  are the permanent magnetic flux for each phase.

Magnetic flux of the rotor generated by permanent magnets in (2.13) is detailed as:

$$\begin{bmatrix} \phi_{pa} \\ \phi_{pb} \\ \phi_{pc} \end{bmatrix} = \phi_m \times \begin{bmatrix} \cos(\theta) \\ \cos(\theta + 120^\circ) \\ \cos(\theta - 120^\circ) \end{bmatrix} \quad (2.14)$$

where,  $\phi_m$  is permanent magnetic flux in stator.

After substituting (2.13) and (2.14) into (2.12), the mathematical model of PMSM in “ABC” stationary reference frame can be expressed as:

$$\begin{bmatrix} u_a \\ u_b \\ u_c \end{bmatrix} = R_s \begin{bmatrix} i_a \\ i_b \\ i_c \end{bmatrix} + \frac{d}{dt} \left\{ \begin{bmatrix} L_{aa} & L_{ab} & L_{ac} \\ L_{ab} & L_{bb} & L_{bc} \\ L_{ac} & L_{bc} & L_{cc} \end{bmatrix} \begin{bmatrix} i_a \\ i_b \\ i_c \end{bmatrix} + \phi_m \begin{bmatrix} \cos(\theta) \\ \cos(\theta + 120^\circ) \\ \cos(\theta - 120^\circ) \end{bmatrix} \right\} \quad (2.15)$$

Time-varying coefficient contained in differential equations of the three phase stationary frame of IPMSM expression making it physically significant. But solving those equations is still a mission impossible. In order to figure out a pattern of motor control and build a reachable mathematical model, establishing new coordinate frame based on the stator or the rotor magnetic field is inevitable. Thus, the mathematical model Typically, a mathematical model after coordinate transformed is easier to be handled.

Transformation (2.10) is valid for any current, voltage and magnetic flux. Applying (2.10) to equation (2.15), a typical IPMSM model in “d-q” rotating frame can be represented as follows.

$$\begin{aligned} V_d &= R_s \cdot i_d - N_p \cdot \omega_r \cdot \phi_q + \dot{\phi}_d \\ V_q &= R_s \cdot i_q - N_p \cdot \omega_r \cdot \phi_d + \dot{\phi}_q \end{aligned} \quad (2.16)$$

$$\begin{aligned} \phi_d &= L_d \cdot i_d + \phi_m \\ \phi_q &= L_q \cdot i_q \end{aligned} \quad (2.17)$$

Utilizing (2.16) and (2.17) d-q axis voltage equations can be rewritten as:

$$\begin{aligned} V_d &= R_s \cdot i_d - N_p \cdot \omega_r \cdot L_q \cdot i_q + \frac{d}{dt} \cdot L_d \cdot i_d \\ V_q &= R_s \cdot i_q - N_p \cdot \omega_r \cdot L_d \cdot i_d + \omega_r \cdot \phi_m + \frac{d}{dt} \cdot L_q \cdot i_q \end{aligned} \quad (2.18)$$

Equivalent circuits is widely applied in system study especially in malfunction detection. Equation (2.18) may be visualized in figure (2.3) and (2.4). Which are known as d-q axis equivalent circuits, respectively. Noted that iron losses is omitted in the circuits. Iron resistance will connected in parallel with equivalent voltage sources if iron losses need to be considered.

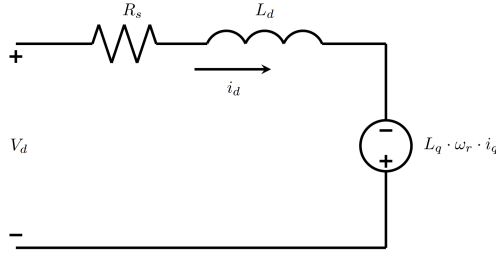


**Figure 2.3:** Motor d-axis equivalent circuit

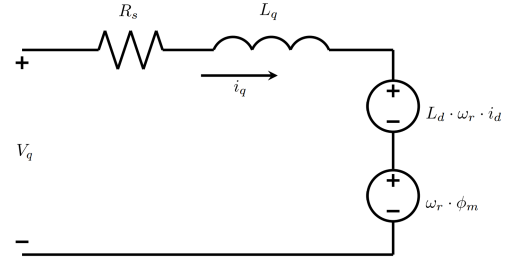


**Figure 2.4:** Motor q-axis equivalent circuit

For the mechanical part of the motor, its characteristic can be defined as:

$$\dot{\omega}_r = \frac{\tau_e - \tau_L - B_m \cdot \omega_r}{J} \quad (2.19)$$

where, the electromagnetic torque is defined as:

$$\tau_e = \frac{3}{2} \cdot N_p \cdot (L_d - L_q) \cdot i_d \cdot i_q + \frac{3}{2} \cdot N_p \cdot \phi_m \cdot i_q \quad (2.20)$$

Thus, re-arranging equations (2.18) and (2.19), the final state space represen-

tation of IPMSM machine can be written as:

$$\begin{aligned} \dot{i}_d &= \frac{1}{L_d} \cdot (-R_s \cdot i_d + N_p \cdot L_q \cdot \omega_r \cdot i_q + V_d) \\ \dot{i}_q &= \frac{1}{L_q} \cdot (-R_s \cdot i_q - N_p \cdot L_d \cdot \omega_r \cdot i_d - N_p \cdot \phi_m \cdot \omega_r + V_q) \\ \dot{\omega}_r &= \frac{3 \cdot N_p \cdot (L_d - L_q)}{2 \cdot J} \cdot i_d \cdot i_q + \frac{3 \cdot N_p \cdot \phi_m}{2 \cdot J} \cdot i_q - \frac{B_m}{J} \cdot \omega_r - \frac{\tau_L}{J} \end{aligned} \quad (2.21)$$

The basic vector diagram of IPMSM is illustrated in Fig.2.5. When constant torque control algorithm is applied, assumption of is taken. With this assumption the phasor diagram is shown in Fig.2.6. The developed torque is only relevance to q-axis current and hence, can be controlled by  $i_q$  when  $i_d = 0$ .

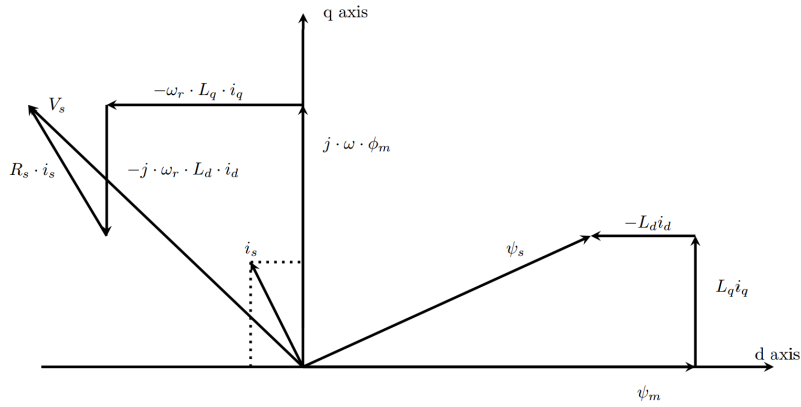


**Figure 2.5:** General IPMSM phasor diagram.

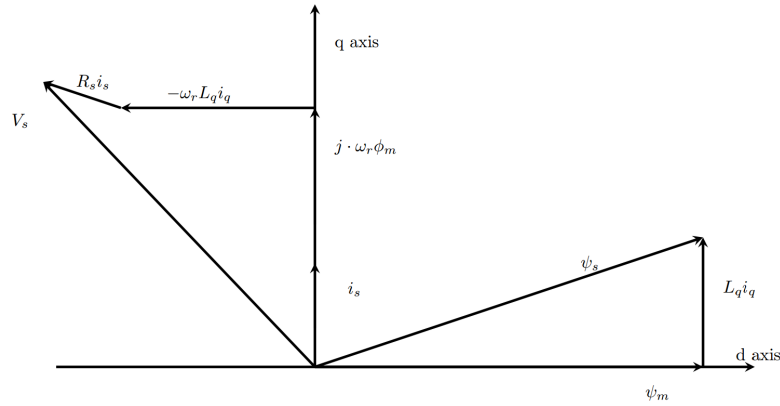


**Figure 2.6:** Phase diagram with  $i_d \equiv 0$  scenario.

## 2.4 Conclusion

On the way of developing mathematical model it is found that the system is a time-varying, multiple variables, nonlinear and highly coupled system. Coordinate transformations decouple the magnetic flux part and torque part to eliminate the difficulty of controller design. The transformation from stationary “ABC” from rotating “d-q” frame of IPMSM mathematical model simplified the system analyzation. By setting d-axis alien with the rotor magnetic flux, winding on d-axis is equivalent to excitation winding on DC motor and winding on q-axis can be seen as armature winding. At this time, d-axis used to control magnetic flux while q-axis used for torque regulation. Thus, the control of IPMSM become similar to separately excited DC motor while it maintains its general advantages over DC motor.

# Chapter 3

## $H_\infty$ Controller for IPMSM Drive

### 3.1 Introduction

Due to the special characteristics of IPMSM, control technique plays an irreplaceable role to achieve dynamic response and excellent performance, insensitive to external load and parameter perturbation. However, neither classic control algorithm nor modern control techniques represented by optimal control all based on deterministic and precise mathematical express could not produce satisfying results in industrial. Robust control put uncertainties into consideration in preliminary controller design stage which makes up the deficiency of traditional theory. Not only it can be utilized in single-input, single-output (SISO) system, but also shows its ability in multiple-input, multiple-output (MIMO) scenario.

Coping with system uncertainty is critical for robust performance. According to characteristics of uncertainties, it could be classified as structured uncertainty and unstructured uncertainty. Structured uncertainty indicates that experts already aware of the location of uncertainties, such as parameters uncertainty, uncertain elements in state space matrix, and zeros and poles uncertainty in transfer functions,

etc. For unpredictable uncertainty like high frequency non-modelled structure or load perturbation are called unstructured uncertainty in general. As a robust controller, an  $H_\infty$  controller will be developed for IPMSM drive. The detail derivation of the proposed  $H_\infty$  controller is provided below. A comprehensive analyze will expressed in this chapter. Based on IPMSM, a proposed  $H_\infty$  controller will be derived.

## 3.2 Preliminary Theory

### 3.2.1 Riccati Equation and Hamiltonian Matrix

Let  $A$ ,  $Q$ ,  $R$  be real  $n \times n$  matrices and  $Q$ ,  $R$  are symmetrical, Hamiltonian matrix  $H \in R^{2n \times 2n}$  is defined as

$$H = \begin{bmatrix} A & -R \\ -Q & -A^T \end{bmatrix} \quad (3.1)$$

Equation about  $X \in R^{n \times n}$

$$X \cdot A + A^T \cdot X - X \cdot R \cdot X + Q = 0 \quad (3.2)$$

named as Riccati equation. And obviously,  $H \in R^{2n \times 2n}$ . For matrix  $X$  which satisfied Riccati equation (3.2) and stabilize  $(A - R \cdot X)$ , represented as  $X = Ric(H)$ . And the domain of  $Ric$  denoted  $dom(Ric)$ .

### 3.2.2 $H_\infty$ norm

$H_\infty$  control theory optimize  $H_\infty$  norms of certain performance specifications in Hardy Spaces (analytic and bonded in the right half plane of complex frequency

domain) to approach robustness controllers. For a right half plane analytic rational function matrix,  $H_\infty$  norm is defined in equation (3.3), and its proof is referred in [63].

$$\|G\|_\infty = \sup_{\text{Re}(s)>0} \bar{\sigma}[G(s)] = \sup_{\omega \in R} \bar{\sigma}[G(j\omega)] \quad (3.3)$$

Where  $G$  is function matrix and  $\bar{\sigma}$  denotes the maximum singular value. The term ‘‘sup’’ can be interpreted as the upper bound of  $\|G(s)\|_\infty$  in frequency domain. For scalar system,  $\|G\|_\infty$  is the peak value of magnitude of amplitude-frequency curve and the maximum distance to origin in phase diagram. Physical meaning of  $H_\infty$  norm represent the maximum energy from input to output that system could obtain.

### 3.2.3 IPMSM Modelling in Frequency Domain

This thesis utilized constant torque control algorithm and based on (2.21), mathematical model under ‘‘ $i_d = 0$ ’’ condition that can be expressed as,

$$\begin{aligned} V_d &= -N_p \cdot \omega_r \cdot L_q \cdot i_q \\ V_q &= R_s \cdot i_q + N_p \cdot \omega_r \cdot \phi_m + L_q \cdot \frac{di_q}{dt} \\ \dot{\omega}_r &= \frac{3 \cdot N_p \cdot \phi_m}{2 \cdot J} \cdot i_q - \frac{B_m}{J} \cdot \omega_r - \frac{\tau_L}{J} \end{aligned} \quad (3.4)$$

Thus, the corresponding block diagram is shown below.

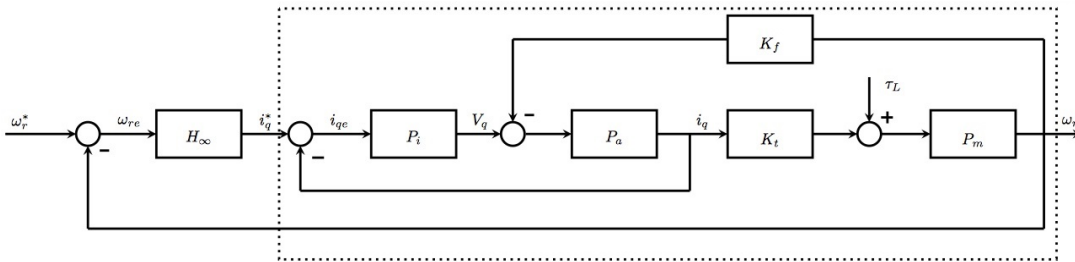
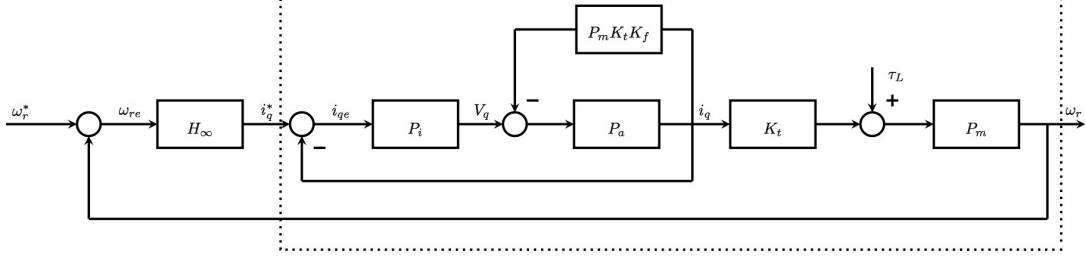


Figure 3.1: Block diagram of  $H_\infty$  based IPMSM.

In order to derive the transfer function  $P(s)$  which is surrounded by the dotted line in Fig.3.1, following simplification of the previous block diagram can be done.



**Figure 3.2:** Simplified Block diagram of Fig. 3.1.

The transfer function block of  $H_\infty$  controller is going to be derived in the related section. The transfer functions for all other blocks in Fig.3.2 can be represented as,

$$\begin{aligned}
 P_i &= \frac{s \cdot k_p + k_i}{s} & P_a &= \frac{1}{s \cdot L_q + R_s} & K_t &= \frac{3}{2} \cdot N_p \cdot \phi_m \\
 K_f &= N_p \cdot \phi_m & P_m &= \frac{1}{s \cdot J + B_m}
 \end{aligned}$$

So, the transfer function can be expressed as,

$$\begin{aligned}
 P(s) &= \frac{\omega_r(s)}{i_q^*(s)} = \frac{K_t \cdot P_m \cdot P_i \cdot P_a}{1 + P_i \cdot P_a + P_m \cdot K_t \cdot K_f \cdot P_a} \\
 &= \frac{s \cdot k_p \cdot k_t + k_i \cdot K_t}{L_q J \cdot s^3 + (B_m L_q + J R_s + J k_p) \cdot s^2 + (R_s B_m + B_m k_p + J k_i + K_t K_f) \cdot s + B_m k_i}
 \end{aligned} \tag{3.5}$$

Transfer function  $P(s)$  will be used in the following subsection when deriving proposed argumentation transfer function matrix  $G(s)$ .

### 3.2.4 Standard $H_\infty$ Output Feedback Control

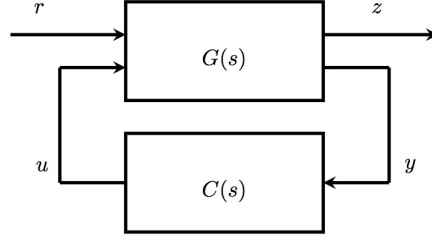


**Figure 3.3:** Standard  $H_\infty$  control system.

Standard  $H_\infty$  control problem is shown in Fig.3.3. Where “ $G(s)$ ” stands for generalized plant containing all the weighting functions. And “ $C(s)$ ” represents designed controller. Symbols “ $r$ ”, “ $u$ ”, “ $z$ ”, “ $y$ ” represents external input (including disturbances, noise and reference signal), control input, error signal and measured signal respectively. Assume  $G(s)$  and  $C(s)$  are rational, real and proper transfer function matrices. Considering the situation in Fig.3.3, one can get,

$$\begin{bmatrix} z \\ y \end{bmatrix} = G(s) \cdot \begin{bmatrix} r \\ u \end{bmatrix} \quad (3.6)$$

where  $G(s)$  is defined as,

$$G(s) = \left[ \begin{array}{c|cc} A & B_1 & B_2 \\ \hline C_1 & D_{11} & D_{12} \\ C_2 & D_{21} & D_{22} \end{array} \right] \quad (3.7)$$

Also  $G(s)$  could be decomposed as,

$$G(s) = \begin{bmatrix} G_{11}(s) & G_{12}(s) \\ G_{21}(s) & G_{22}(s) \end{bmatrix} \quad (3.8)$$

Again  $C(s)$  is defined as,

$$C(s) = \left[ \begin{array}{c|c} A_C & B_C \\ \hline C_C & D_C \end{array} \right] \quad (3.9)$$

Combining equations (3.7) and (3.8) yields

$$G_{ij}(s) = C_i \cdot (s \cdot I - A)^{-1} \cdot B_j + D_{ij}, \quad i, j = 1, 2 \quad (3.10)$$

The closed-loop transfer function from “ $r$ ” to “ $z$ ” in Fig.3.3 can be derived as

$$T_{zr} = G_{11}(s) + G_{12}(s) \cdot C(s) \cdot (I - G_{22}(s) \cdot C(s))^{-1} \cdot G_{21}(s) \quad (3.11)$$

The process above also referred to as a lower Linear Fractional Transformation (LFT) on  $C(s)$ .

Following two theorems give out the definition of  $H_\infty$  optimal control and sub-optimal control.

*$H_\infty$  Optimal Control:* For the system in Fig.3.3, find a rational, real and proper controller  $C(s)$  which internally stabilizes the closed loop system and minimize the value of  $\gamma$ , so that  $\|T_{zr}\|_\infty$ .

For generalized model  $G(s)$  in (3.7), the following assumptions are made [24].

- (1)  $(A, B_1)$  stabilizable and  $(C_1, A)$  detectable;
- (2)  $(A, B_2)$  stabilizable and  $(C_2, A)$  detectable;
- (3)  $D_{12}^T \cdot \begin{bmatrix} C_1 & D_{12} \end{bmatrix} = \begin{bmatrix} 0 & I \end{bmatrix}$ ;
- (4)  $\begin{bmatrix} B_1 & D_{21} \end{bmatrix}^T \cdot D_{21}^T = \begin{bmatrix} 0 & I \end{bmatrix}^T$ ;
- (5)  $D_{11} = 0, D_{22} = 0$ ;

Those assumptions simplify the theorem statements and proofs. Where assump-

tion (1) together with (2) is the necessary and sufficient conditions for generalized system internally stable. Assumptions (3) and (4) concerns impact from external signal  $r$  entering  $G(s)$ , and minimize the infinity norm of the closed-loop transfer function  $r$  to  $z$ ,  $\|T_{rz}\|_\infty$ . Condition (5) is used for the sake of simplifying the  $H_\infty$  controller. When condition (3) - (5) are not satisfied, modifications can be done for  $G(s)$  to meet the conditions.

Solutions for  $H_\infty$  optimal controllers involve two Hamiltonian matrices.

*Theorem [24]:* For closed-loop system in Fig.3.3, consider generalized system (3.7) and controller (3.9). The controller  $C(s)$  exists, stabilize the closed-loop system and minimize  $\|T_{zw}\|_\infty$  if and only if all the following conditions hold.

(1) For Hamiltonian matrix

$$H_\infty = \begin{bmatrix} A & \gamma^{-2}B_1B_1^T - B_2B_2^T \\ -C_1C_1^T & -A^T \end{bmatrix} \quad (3.12)$$

where,  $H_\infty \in \text{dom}(Ric)$ ,  $X_\infty = Ric(H_\infty) \geq 0$

(2) For another Hamiltonian matrix

$$J_\infty = \begin{bmatrix} A^T & \gamma^{-2}C_1^TC_1 - C_2^TC_2 \\ -B_1B_1^T & -A \end{bmatrix} \quad (3.13)$$

where,  $J_\infty \in \text{dom}(Ric)$ ,  $Y_\infty = Ric(H_\infty) \geq 0$

$$(3)\rho \begin{pmatrix} X_\infty & Y_\infty \end{pmatrix} < 0$$

where,  $\rho \begin{pmatrix} X_\infty & Y_\infty \end{pmatrix}$  is spectral radius of  $X_\infty$  and  $Y_\infty$ , indicating maximum amplitude of their singular value.

According to the discussion in equations (3.1) and (3.2). For (3.12) and (3.13), there exist a semi positive definite solution for  $X_\infty$  and  $Y_\infty$  satisfying

the following Riccati equations and stabilize  $A + (\gamma^{-2}B_1B_1^T - B_2B_2^T) \cdot X_\infty$  and  $A^T + (\gamma^{-2}C_1^TC_1 - C_2^TC_2) \cdot Y_\infty$ , respectively.

$$\begin{aligned} X_\infty A + A^T X_\infty + X_\infty (\gamma^{-2}B_1B_1^T - B_2B_2^T) X_\infty + C_1^T C_1 &= 0 \\ AY_\infty + Y_\infty A^T + Y_\infty (\gamma^{-2}C_1^T C_1 - C_2^T C_2) Y_\infty + B_1 B_1^T &= 0 \end{aligned} \quad (3.14)$$

The  $H_\infty$  output controller can be defined as,

$$C(s) = \begin{bmatrix} A_\infty & -Z_\infty L_\infty \\ F_\infty & 0 \end{bmatrix} \quad (3.15)$$

where,

$$\begin{aligned} A_\infty &= A + \gamma^{-2}B_1B_1^T X_\infty + B_2 F_\infty + Z_\infty L_\infty C_2 \\ F_\infty &= -B_2^T X_\infty \\ L_\infty &= -Y_\infty C_2^T \\ Z_\infty &= (I - \gamma^2 Y_\infty X_\infty)^{-1} \end{aligned}$$

### 3.3 $H_\infty$ controller with Mixed-sensitivity Approach

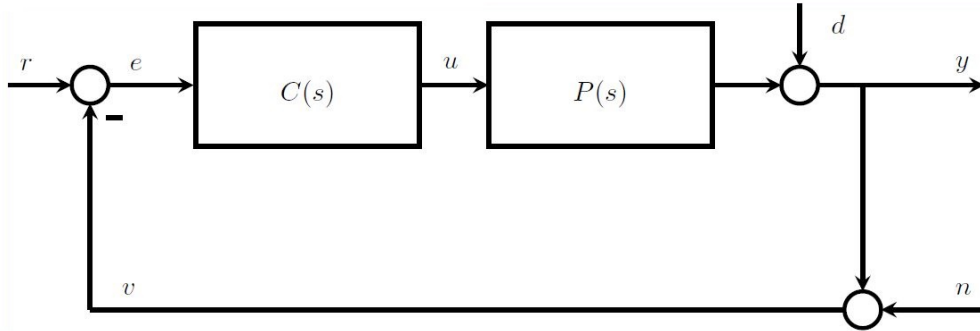


Figure 3.4: A basic feedback control system.

Fig.3.4 shows a basic feedback system loop. In this section the corresponding sensitivity function and complementary sensitivity function will be derived. And

from this figure, the following relations can be easily found.

$$\begin{aligned}
 S(s) &= \frac{e}{r} = \frac{d}{y} = \frac{I}{I + P(s) \cdot C(s)} \\
 T(s) &= \frac{y}{r} = \frac{P(s) \cdot C(s)}{I + P(s) \cdot C(s)} \\
 R(s) &= \frac{u}{r} = \frac{C(s)}{I + P(s) \cdot C(s)}
 \end{aligned} \tag{3.16}$$

Where  $S(s)$  and  $T(s)$  represent the sensitivity and complementary sensitivity function, respectively. Sensitivity function reflects the relationship between error signal and reference signal along with the connection in disturbance signal and feedback signal. Smaller  $S(s)$  indicates that the closed-loop system has better performance in tracking command signal and attenuating disturbance. While the  $T(s)$  defined as the transfer function from feedback signal to reference signal. In order to eliminate the influence from unstructured model and make the system robust and stable, a smaller  $T(s)$  is also desired. However, the summation of  $S(s)$  and  $T(s)$  is constantly equal to 1.

$$\begin{aligned}
 S(s) + T(s) &= \frac{e}{r} + \frac{y}{r} = \frac{e + v}{r} = \frac{r - v + v}{r} \\
 &= \frac{I}{I + P(s) \cdot C(s)} + \frac{P(s) \cdot C(s)}{I + P(s) \cdot C(s)} \\
 &= 1
 \end{aligned} \tag{3.17}$$

Which means a compromise must be made carefully between  $S(s)$  and  $T(s)$ . Thus, this approach is called mixed sensitivity approach.  $R(s)$  represents the transfer function from reference signal to control input. It helps the system in getting the correct control signal. The detailed transfer functions determined by weight functions will be illustrated in the following section.

### 3.4 Mixed-Sensitivity Based $H_\infty$ Controller for IPMSM

Previous sections provided the nominal plant  $P(s)$  for IPMSM and standard  $H_\infty$  control algorithm. This section will focus on converting IPMSM speed tracking problem to standard  $H_\infty$  problem.

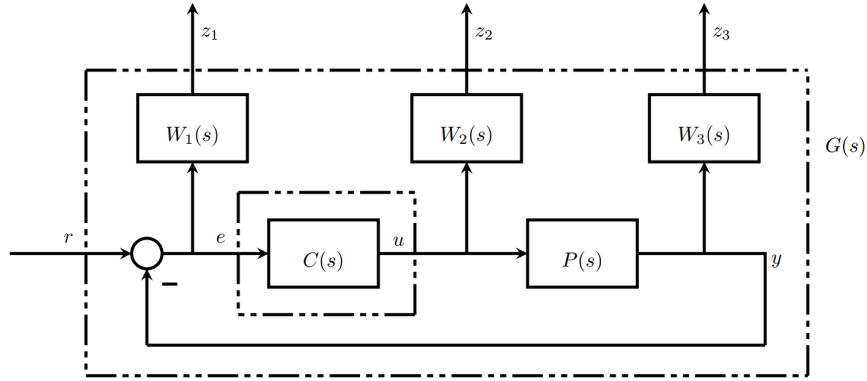


**Figure 3.5:** Block diagram of  $H_\infty$  mixed sensitivity

According to discussions above, three sensitivity functions are defined. Fig.3.5 adds  $S(s)$ ,  $R(s)$  and  $T(s)$  along with their weight functions  $W_1$ ,  $W_2$  and  $W_3$  into Fig.3.4. To be noticed, measured signal  $z$  is treated as a matrix  $\begin{bmatrix} z_1 & z_2 & z_3 \end{bmatrix}^T$ . The area surrounded by dash-line is referred as the generalized plant  $G(s)$  after augmentation from  $P(s)$ .

Comparing Fig.3.5 and Fig.3.3, consider “ $r$ ” and “ $u$ ” as input signals while “ $z_1$ ”, “ $z_2$ ”, “ $z_3$ ” and “ $e$ ” as output signal, the following equation can be obtained.

$$\begin{bmatrix} z_1 \\ z_2 \\ z_3 \\ e \end{bmatrix} = G(s) \cdot \begin{bmatrix} r \\ u \end{bmatrix} \quad (3.18)$$

From Fig.3.5, the augmented plant can be derived as:

$$G(s) = \left[ \begin{array}{c|c} W_1(s) & -W_1(s) \cdot P(s) \\ \hline 0 & W_2(s) \\ 0 & W_3(s) \cdot P(s) \\ \hline I & -P(s) \end{array} \right] \quad (3.19)$$

Thus, each sub-matrix in (3.8) can be denoted as:

$$\begin{aligned} G_{11}(s) &= \begin{bmatrix} W_1(s) \\ 0 \\ 0 \end{bmatrix} & G_{12}(s) &= \begin{bmatrix} -W_1(s) \cdot P(s) \\ W_2(s) \\ W_3(s) \cdot P(s) \end{bmatrix} \\ G_{21}(s) &= I & G_{22}(s) &= -P(s) \end{aligned} \quad (3.20)$$

Recall the definition about  $H_\infty$  optimal control in previous section. The block diagram of three transfer functions are shown in Fig.3.6.

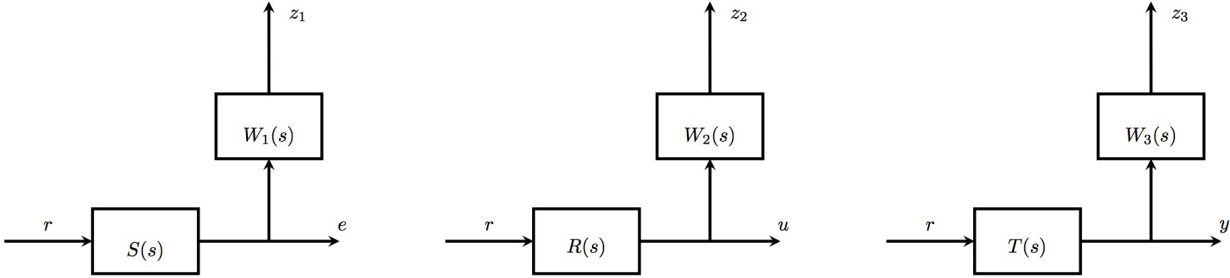


**Figure 3.6:** Block diagram for every sensitivity function

Minimization of the infinity norm of transfer functions  $T_{z_1 r}$ ,  $T_{z_2 r}$  and  $T_{z_3 r}$  are equivalent to the minimization of the infinity norm of overall transfer function  $T_{zr}$ .

Thus,

$$\|T_{zr}\|_\infty = \left\| \begin{bmatrix} T_{z1r} \\ T_{z2r} \\ T_{z3r} \end{bmatrix} \right\|_\infty = \left\| \begin{bmatrix} W_1 \cdot S \\ W_2 \cdot R \\ W_3 \cdot T \end{bmatrix} \right\|_\infty \quad (3.21)$$

### 3.4.1 Weight Function Selection and Controller Design

Proper weight function is an important step in  $H_\infty$  controller design. To a large degree, feasible controller performance depends on weight functions. For different application and different system model, the weight function will be different. Its selection does not have a consistent method and reason, mainly based on some empirical principles.  $H_\infty$  optimal controller could be derived after several experiential attempts.

#### A. Selection of $W_1$

$W_1$  used for penalizing the error signal and weighting the sensitivity function  $S(s)$ . It represents frequency characteristics about disturbance, shows the requirement on sensitivity function. From equation (3.16),  $S(s)$  represents the relation between command signal and tracking error as well as output signal and disturbance input. In most cases, low frequency is one of the features for above signals. In low frequency band, to reduce disturbance affection and improve tracking ability, the gain of sensitivity function is demanded as low as possible, requiring  $W_1$  working as a low-pass filter. Meaning that low frequency gain of  $W_1$  should be greater than command-error ratio for disturbance attenuation and reference tracking ability. For high frequency band, there is no special requirement about the shape of  $W_1$ . The necessary and sufficient condition for  $S(s)$  can be expressed as,

$$\bar{\sigma}(S(s)) \leq \underline{\sigma}(W_1^{-1}(s)) \quad (3.22)$$

Overall,  $W_1$  has high gain and low pass features.

### B. Selection of $W_2$

$W_2$  is used for penalizing the control signal and weighting additive perturbation. Transfer function  $R(s)$  denotes the relation between reference input and control input,  $W_2$  limiting control input and remaining it in allowed range to prevent saturation damage the system. From this prospective,  $W_2$  should be large. However,  $W_2$  also have positive effect on system band width,  $W_2$  should be small enough to ensure sufficient bandwidth. For the sake of controller simplicity and reducing controller order,  $W_2$  can be choose as a constant value to represent additive perturbation boundary. From (3.21) the necessary and sufficient condition for  $R(s)$  can be expressed as,

$$\bar{\sigma}(R(s)) \leq \underline{\sigma}(W_2^{-1}(s)) \quad (3.23)$$

### C. Selection of $W_3$

$W_3$  is used for penalizing the output signal and weighting complementary sensitivity function  $T(s)$ , representing the boundary of multiplicative perturbation. Mathematical model describes low frequency characteristics of objective system. Due to non-modelled high frequency characteristics, mathematical model couldn't contain all the information that real-time has. This non-modelled part is because of ignored factors, some of them were neglected for simplicity, the others due to human limited ability. Thus, commonly use multiplicative perturbation to cover those influence. To endure high frequency uncertainty, smaller complementary sensitive function  $T(s)$  required. But, as the discussion shown in equation (3.16), due to  $S(s) + T(s) = I$ , compromise has be made between  $W_1(s)$  and  $W_2(s)$  for low frequency disturbance attenuation and high frequency uncertainty attenuation.

From (3.21) following inequality can be obtained.

$$\bar{\sigma}(T(s)) \leq \underline{\sigma}(W_3^{-1}(s)) \quad (3.24)$$

To meet the requirement of  $S(s) + T(s) = 1$ ,  $W_3$  also hold the following equation.

$$\bar{\sigma}(W_1^{-1}(s)) + \bar{\sigma}(W_3^{-1}(s)) \geq 1 \quad (3.25)$$

Usually cut off frequency of  $W_3$  is set as greater than  $W_1$  to meet this criteria.

## 3.5 Conclusion

This chapter designs robust  $H_\infty$  controller based on mixed-sensitivity method. Preliminary mathematical theory about norms and Riccati equation were given. Then, the standard  $H_\infty$  control algorithm and its controller derivation based on the solutions of two Riccati equations were provided. From small-gain theory, system stability was verified. For the system in this thesis, a conversion from standard  $H_\infty$  to mixed-sensitivity were also detailed. This Chapter also focused on the weight function determination with detailed reasons and processes. Simulation and real-time verification about feasibility will be considered in following Chapters.

# Chapter 4

## Nonlinear PCHD Controller for IPMSM Drive

### 4.1 Introduction

A mechanical system is stable if and only if its kinetic and potential energy are approaching to zero. Meaning that whether the system have external energy injected or not, the system only consume energy but not exporting them back. In other words, the system will not amplify the injected energy and it will be stabilize. When the internal energy gets depleted, the energy import is stopped. Thus, a positive definite function that represents total system energy have been analyzed. All state variables approaching to zero are the sufficient and necessary condition for stabilizing this system. Passivity and dissipativity are two necessary theories to be introduced in order to analyze system's stability and how it will response to externally injected energy. Consider the non-linear dynamic system

and output described by the following differential equations:

$$\begin{aligned}\dot{x} &= f(x) + g(x) \cdot u \\ y &= h(x)\end{aligned}\tag{4.1}$$

where,  $x \in R^n$  for state variables,  $u \in R^n$ ,  $y \in R^n$  are denoted as control input signal and output signal with the same dimension  $n$ .

**Theorem 4.1** *The control system (4.1) is said to be dissipative with respect to the supply rate  $s(u, y)$ , if there exists a positive semi-definite storage function  $V(x)$  such that the dissipation inequality*

$$V(x(T)) - V(x(0)) \leq \int_0^T s(u, y) dt\tag{4.2}$$

is satisfied for all  $T > 0$ .  $V(x)$  named as energy storage function and (4.2) is called dissipation inequality [64].

Furthermore, if a positive definite function  $Q(x) > 0$  exists for

$$V(x(T)) + \int_0^T Q(x) dt \leq V(x(0)) + \int_0^T s(u, y) dt\tag{4.3}$$

Then the system is strictly dissipative.

System's total initial energy is represented as  $V(x(0))$ , and  $V(x(T))$  stands for total energy at any time  $T$ . Therefore, left side of (4.2) shows the energy changes of the system internally from time 0 to  $T$ . While the right side of the inequality indicates how much energy was injected to the system externally from time 0 to  $T$ . This analysis proved that dissipativeness is closely related to system energy. Physically speaking, from time  $T$  to initial state, external injected energy is always greater or equal to energy gain of system itself. So for a dissipative

system, its movement is always accompanied with energy consumption.

The significance of dissipation is that it has a intimate relation with stability. For (4.3), if the energy supply rate  $s(u, y) = 0$ , the system does not absorb any energy from outside. The derivative of equation (4.3) yields,

$$\dot{V} \leq s(u, y) - Q(x) \leq -Q(x) < 0, \quad \forall x \neq 0 \quad (4.4)$$

The first order derivative of energy storage function is negative definite, according to Lyapunov stability theory, the system is asymptotically stable at  $x = 0$ .

This chapter utilizes energy formulations in controller design, rendering selected energy formulation that can reflect system's internal structure and dynamic information. In fact, many industrial dynamic model is based on energy relationship. In this thesis Hamiltonian system is utilized for such relationship to develop the dynamic model of the IPMSM.

## 4.2 Port Controlled Hamiltonian with Dissipation System

Researches on mechanical system usually based on Euler-Lagrange equation, which is derived from d'Alembert principle [65]:

$$\frac{d}{dt} \left( \frac{\partial L}{\partial \dot{q}_i} \right) - \frac{\partial L}{\partial q_i} = \tau_i \quad i = 1, 2 \cdots n \quad (4.5)$$

where  $q_i = \begin{bmatrix} q_1 & q_2 & \cdots & q_n \end{bmatrix}^T$  is  $n$  dimensional generalized displacement vector.

Obviously, its first-order derivative  $\dot{q}_i = \begin{bmatrix} \dot{q}_1 & \dot{q}_2 & \cdots & \dot{q}_n \end{bmatrix}^T$  is generalized speed.

While  $\tau_i = \begin{bmatrix} \dot{\tau}_1 & \dot{\tau}_2 & \cdots & \dot{\tau}_n \end{bmatrix}^T$  is denoted as  $n$  dimensional generalized forces. Symbol  $L$  is defined as the difference between kinetic energy and potential energy ( $L(q, \dot{q}) = T(q, \dot{q}) - P(q)$ ). Kinetic energy in mechanical system is defined as,

$$T(q_i, \dot{q}_i) = \frac{1}{2} \dot{q}_i^T M(q_i) \dot{q}_i \quad (4.6)$$

where  $M(q_i)$  is  $n$  dimensional generalized mass. Thus,

$$L(q_i, \dot{q}_i) = \frac{1}{2} \dot{q}_i^T M(q_i) \dot{q}_i - P(q_i) \quad (4.7)$$

Defining a generalized momentum vector  $p_i = \begin{bmatrix} p_1 & p_2 & \cdots & p_n \end{bmatrix}^T = M(q_i) \dot{q}_i$  to replace  $\dot{q}_i$  in (4.7) yields,

$$L(q_i, p_i) = \frac{1}{2} p_i^T M^{-1}(q) p_i - P(q_i) \quad (4.8)$$

Lagrangian formulation describes system kinematics from displacement and speed, while Hamiltonian formulations are utilizing displacement and momentum. In mechanical system, Legendre transformation [66] are used to derive Hamiltonian formulation from the Lagrangian formulation by coordinate transformation, which is defined as:

$$H(q_i, p_i) = \dot{q}_i^T p_i - L(q_i, \dot{q}_i) \quad (4.9)$$

Combining (4.9) and (4.8), system total energy is given by,

$$H(q_i, p_i) = \frac{1}{2} p_i^T M^{-1}(q) p_i + P(q_i) \quad (4.10)$$

Thus, the new coordinate frame  $(q, p)$  and Hamiltonian function  $H(q_i, p_i)$  could express Euler-Lagrange equation (4.5) as,

$$\begin{aligned}\dot{q}_i &= \frac{\partial H}{\partial p_i} \\ \dot{p}_i &= -\frac{\partial H}{\partial q_i} + u\end{aligned}\tag{4.11}$$

In matrix form, (4.11) can be written as,

$$\begin{bmatrix} \dot{q}_i \\ \dot{p}_i \end{bmatrix} = J \cdot \begin{bmatrix} \frac{\partial H}{\partial p_i} \\ \frac{\partial H}{\partial q_i} \end{bmatrix} + g \cdot u\tag{4.12}$$

where

$$J = \begin{bmatrix} 0 & I \\ -I & 0 \end{bmatrix}, \quad g = \begin{bmatrix} 0 \\ I \end{bmatrix}$$

Eqn.(4.12) is named as Hamiltonian formulation. Two characteristics can be summarized based on a comparison with (4.5). Firstly, (4.12) has affine nonlinear structure and secondly, Hamiltonian function is the summation of kinetic and potential energy, which is the total energy of the system. Furthermore, the Hamiltonian system output is defined as,

$$y = \frac{\partial H(q_i, p_i)}{\partial p_i} = \dot{q}_i\tag{4.13}$$

Consider the Hamiltonian differential equation with respect to time  $t$  as,

$$\begin{aligned}
\frac{dH(q, p)}{dt} &= \begin{bmatrix} \frac{\partial^T H}{\partial q_i} & \frac{\partial^T H}{\partial p_i} \end{bmatrix} \begin{bmatrix} \dot{q}_i \\ \dot{p}_i \end{bmatrix} \\
&= \begin{bmatrix} \dot{q}_i \\ \dot{p}_i \end{bmatrix} \left( J \cdot \begin{bmatrix} \frac{\partial H}{\partial p_i} \\ \frac{\partial H}{\partial q_i} \end{bmatrix} + g \cdot u \right) \\
&= \begin{bmatrix} \frac{\partial^T H}{\partial q_i} & \frac{\partial^T H}{\partial p_i} \end{bmatrix} \cdot g u \\
&= \frac{\partial^T H}{\partial p} \cdot u
\end{aligned} \tag{4.14}$$

Then, Hamiltonian formulation satisfy the following dissipation inequality,

$$\dot{H}(q_i, p_i) \leq y^T u = \dot{q}_i^T u \tag{4.15}$$

Thus, the Hamiltonian system is a passive type. Extending the above system to local coordinate, (4.12) can be expressed in the following form which is called port controlled Hamiltonian system (PCH).

$$\begin{aligned}
\dot{x} &= f(x) + g(x) \cdot u = J(x) \cdot \frac{\partial H(x)}{\partial x} + g(x) \cdot u \\
y &= h(x) = g^T(x) \cdot \frac{\partial H(x)}{\partial x}
\end{aligned} \tag{4.16}$$

Resistive elements that dissipate energy is added into PCH system, which is known as port controlled Hamiltonian with dissipation (PCHD) system.

$$\begin{aligned}
\dot{x} &= [J(x) - R(x)] \cdot \frac{\partial H(x)}{\partial x} + g(x) \cdot u \\
y &= g^T(x) \cdot \frac{\partial H(x)}{\partial x}
\end{aligned} \tag{4.17}$$

where  $x \in R^n$  is state variable and  $u$  for command input signal. Hamiltonian function  $H(x)$  is semi-positive definite. Two indispensable components  $J(x)$  and  $R(x)$  reflect system's internal interconnection structure and damping structure, respectively. In addition,  $J(x)$ ,  $R(x)$  should satisfied following conditions.

$$\begin{aligned} J(x) &= -J^T(x) \\ R(x) &= -R^T(x) \geq 0, \quad \forall x \end{aligned} \tag{4.18}$$

Using (4.17), the derivative of  $H(x)$  with respect to time  $t$  can be written as,

$$\begin{aligned} \frac{dH(x)}{dt} &= \frac{\partial^T H}{\partial x} \left\{ (J(x) - R(x)) \cdot \frac{\partial H}{\partial x} + g(x) \cdot u \right\} \\ &= \frac{1}{2} \cdot \frac{\partial^T H}{\partial x} \{ J(x) + J^T(x) \} \frac{\partial H}{\partial x} - \frac{\partial^T H}{\partial x} \cdot R(x) \cdot \frac{\partial H}{\partial x} + \frac{\partial^T H}{\partial x} \cdot g(x) \cdot u \\ &= -\frac{\partial^T H}{\partial x} \cdot R(x) \cdot \frac{\partial H}{\partial x} + y^T \cdot u \end{aligned} \tag{4.19}$$

According to semi-positive definite of  $R(x) \geq 0$ , therefore,

$$\frac{dH(x)}{dt} \leq y^T \cdot u \tag{4.20}$$

The system (4.17) is passive and Hamiltonian formulation satisfies dissipation inequality (4.4). To be noticed that, if  $R(x) = 0$ , then Hamiltonian system has only energy internal exchange and no energy losses. Thus,  $R(s)$  usually consisted by energy dissipative components. Therefore, (4.17) draw an outline of mathematical expression of a system internally and externally, and delineate a way of energy exchange.

**Theorem 4.2** *If the system described in (4.17) is passive and zero-detectable, and when input  $u$  is negative feedback such as,*

$$u = -y = -g^T(x) \cdot \frac{\partial H(x)}{\partial x} \quad (4.21)$$

*Then, the closed-loop system is asymptotically stable in  $x = 0$ .*

However, for most industrial system especially IPMSM utilized in this thesis, desired equilibrium point is not zero, and Hamiltonian function is not minimized at this point either. Proper adjustments for Hamiltonian function and feedback controller are required for desired equilibrium point stabilization.

**Theorem 4.3** *Consider the system (4.17), set  $x_d$  as desired equilibrium point and  $u = \alpha(x)$  as feedback control law,  $J_c(x)$ ,  $R_c(x)$  and  $H_c(x)$  hold for following conditions*

$$\begin{aligned} J_d(x) &= J(x) + J_c(x) = -J_d^T(x) \\ R_d(x) &= R(x) + R_c(x) = R_d^T(x) \geq 0 \\ H_d(x) &= H(x) + H_c(x) \end{aligned} \quad (4.22)$$

*and  $H_c(x)$  is feasible for*

$$g(x) [J_d(x) - R_d(x)] \frac{\partial H_c}{\partial x} = -g(x) [J_c(x) - R_c(x)] \frac{\partial H}{\partial x} + g(x) \alpha(x) \quad (4.23)$$

*Then, the control law which stabilizes the close-loop system at equilibrium point  $x_d$  is defined as,*

$$u = \alpha(x) = (g^T(x) g(x))^{-1} g^T(x) \left\{ [J_d(x) - R_d(x)] \frac{\partial H_c}{\partial x} + [J_c(x) - R_c(x)] \frac{\partial H}{\partial x} \right\} \quad (4.24)$$

Furthermore, if  $x$  is included in set

$$\left\{ x \in R^n \mid \frac{\partial^T H_d}{\partial x} R_d(x) \frac{\partial H_d}{\partial x} = 0 \right\} \quad (4.25)$$

Then the system is asymptotically stable in equilibrium point  $x_d$ .

### 4.3 PCHD Model for IPMSM

Mathematical model for IPMSM has already been derived in Chapter 2. For its PCHD representation, in order to meet the requirement in (4.18), modifications are needed to be done in the first place. From (2.21), the mathematical model of IPMSM is given by,

$$\begin{aligned} \frac{d}{dt} \cdot L_d i_d &= -R_s \cdot i_d + N_p \cdot L_q \cdot \omega_r \cdot i_q + V_d \\ \frac{d}{dt} \cdot L_q i_q &= -R_s \cdot i_q - N_p \cdot L_d \cdot \omega_r \cdot i_d - N_p \cdot \phi_m \cdot \omega_r + V_q \\ \frac{d}{dt} \cdot \frac{2}{3} J \omega_r &= -\frac{2}{3} B_m \cdot \omega_r + N_p \cdot (L_d - L_q) \cdot i_d \cdot i_q + N_p \cdot \phi_m \cdot i_q - \frac{2}{3} \tau_L \end{aligned} \quad (4.26)$$

Consider the state variables and input vectors as follows,

$$\begin{aligned} x &= \begin{bmatrix} x_1 \\ x_2 \\ x_3 \end{bmatrix} = \begin{bmatrix} L_d i_d \\ L_q i_q \\ \frac{2}{3} \cdot J \omega_r \end{bmatrix} \\ u &= \begin{bmatrix} V_d \\ V_q \\ -\frac{2}{3} \tau_L \end{bmatrix} \end{aligned} \quad (4.27)$$

Hamiltonian formulation is set as the total energy summation of electrical energy and mechanical energy.

$$H(x) = \frac{1}{2} \cdot x^T \cdot D^{-1} \cdot x \quad (4.28)$$

$$\frac{\partial H}{\partial x} = D^{-1}x \quad (4.29)$$

Eqn.(4.26) can be rewritten (2.21) in the form of (4.17), IPMSM in PCHD representation can be written in the following form.

$$\begin{aligned} \frac{d}{dt} \begin{bmatrix} L_d i_d \\ L_q i_q \\ \frac{2}{3} J \omega_r \end{bmatrix} &= [J(x) - R(x)] \cdot \begin{bmatrix} i_d \\ i_q \\ \omega_r \end{bmatrix} + g(x) \cdot \begin{bmatrix} V_d \\ V_q \\ -\frac{2}{3} \tau_L \end{bmatrix} \\ y &= g^T(x) \begin{bmatrix} i_d \\ i_q \\ \omega_r \end{bmatrix} \end{aligned} \quad (4.30)$$

where,

$$\begin{aligned} J(x) &= \begin{bmatrix} 0 & 0 & N_p \cdot x_2 \\ 0 & 0 & -N_p \cdot (x_1 + \phi_m) \\ -N_p \cdot x_2 & N_p \cdot (x_1 + \phi_m) & 0 \end{bmatrix} \\ R(x) &= \begin{bmatrix} R_s & 0 & 0 \\ 0 & R_s & 0 \\ 0 & 0 & \frac{2}{3} B_m \end{bmatrix}, \quad g(x) = \begin{bmatrix} 1 & 0 & 0 \\ 0 & 1 & 0 \\ 0 & 0 & 1 \end{bmatrix} \end{aligned} \quad (4.31)$$

Consider the IPMSM system (2.21) needs to be stabilized at equilibrium point  $x^*$ , where  $x^* = \begin{bmatrix} x_1^* & x_2^* & x_3^* \end{bmatrix}^T$ . When IPMSM is utilized the constant torque

angle control algorithm  $i_d^* = 0$ , from (4.26), the equilibrium point for q-axis current can be derived using the speed differential equation as,

$$\frac{2}{3} \cdot J \frac{d\omega_r^*}{dt} = N_p \cdot \phi_m \cdot i_q^* - \frac{2}{3} B_m \omega_r^* - \frac{2}{3} \tau_L^* \quad (4.32)$$

At any steady constant speed,  $\frac{d\omega_r^*}{dt} = 0$ . Thus, the reference of q-axis current derived from (4.32) is given by,

$$i_q^* = \frac{2 \cdot \tau_L^* + 2 \cdot B_m \omega_r^*}{3 \cdot N_p \cdot \phi_m} \quad (4.33)$$

Then  $x^*$  can be denoted as,

$$\begin{aligned} x^* &= \left[ L_d i_d^* \quad L_q i_q^* \quad \frac{2}{3} J \omega_r^* \right]^T \\ &= \left[ 0 \quad \frac{2 \cdot L_q \cdot \tau_L^* + 2 \cdot L_q \cdot B_m \omega_r^*}{3 \cdot N_p \cdot \phi_m} \quad \frac{2}{3} J \omega_r^* \right]^T \end{aligned} \quad (4.34)$$

A feedback closed-loop energy function  $H_d(x)$  is needed to be established, and minimize  $H_d(x)$  at  $x^*$ . In other words, at any time  $t \geq 0$ ,  $H_d(x) > H(x^*)$  holds for  $x \neq x^*$ . In addition, looking for a feedback control law  $u = \alpha(x)$  which stabilizes the closed-loop system to

$$\dot{x} = [J_d(x) - R_d(x)] \cdot \frac{\partial H_d(x)}{\partial x} \quad (4.35)$$

where Hamiltonian formulation for closed-loop is chosen as,

$$H_d(x) = \frac{1}{2} \cdot (x - x^*)^T D^{-1} (x - x^*) \quad (4.36)$$

As discussed above, interconnection matrix represents the system energy trans-

fer internally and damping matrix denotes the energy consumption characteristic.

Without loosing generality, set

$$J_c(x) = \begin{bmatrix} 0 & -J_{12} & J_{13} \\ J_{12} & 0 & -J_{23} \\ -J_{13} & J_{23} & 0 \end{bmatrix}, \quad R_c(x) = \begin{bmatrix} r_1 & 0 & 0 \\ 0 & r_2 & 0 \\ 0 & 0 & r_3 \end{bmatrix} \quad (4.37)$$

where  $J_{11}$ ,  $J_{12}$ ,  $J_{13}$  and  $r_1$ ,  $r_2$ ,  $r_3$  are undetermined parameters. As discussed before, from (4.23) and (4.24),

$$\begin{aligned} & \begin{bmatrix} -R_s - r_1 & -J_{12} & N_p \cdot x_2 + J_{13} \\ J_{12} & -R_s - r_2 & -N_p \cdot (x_1 + \phi_m) - J_{23} \\ -N_p \cdot x_2 - J_{13} & N_p \cdot (x_1 + \phi_m) + J_{23} & -\frac{2}{3}B_m - r_3 \end{bmatrix} \cdot \begin{bmatrix} i_d^* \\ i_q^* \\ \omega_r^* \end{bmatrix} \\ &= \begin{bmatrix} -r_1 & -J_{12} & J_{13} \\ J_{12} & -r_2 & -J_{23} \\ -J_{13} & J_{23} & -r_3 \end{bmatrix} \cdot \begin{bmatrix} i_d \\ i_q \\ \omega_r \end{bmatrix} - \begin{bmatrix} 1 & 0 & 0 \\ 0 & 1 & 0 \\ 0 & 0 & 1 \end{bmatrix} \cdot \begin{bmatrix} u_d \\ u_q \\ -\frac{2}{3}\tau_L \end{bmatrix} \quad (4.38) \end{aligned}$$

In above equation (4.38), system input vector  $\begin{bmatrix} u_d & u_q & -\frac{2}{3}\tau_L \end{bmatrix}^T$  could be expressed as,

$$\begin{aligned} u_d &= -r_1 (i_d - i_d^*) - J_{12} (i_q - i_q^*) - J_{13} (\omega_r - \omega_r^*) + R_s i_d^* - N_p L_q i_q \omega_r^* \\ u_q &= J_{12} (i_d - i_d^*) - r_2 (i_q - i_q^*) - J_{23} (\omega_r - \omega_r^*) + R_s i_q^* + N_p L_d i_d \omega_r^* + N_p \phi_m \omega_r^* \\ \tau_L &= J_{13} (i_d - i_d^*) - J_{23} (i_q - i_q^*) + r_3 (\omega_r - \omega_r^*) - \frac{3}{2} N_p L_q i_q i_d^* + \frac{3}{2} N_p L_d i_d i_q^* + \frac{3}{2} N_p \phi_m i_q^* - B_m \omega_r^* \end{aligned} \quad (4.39)$$

From (4.22) and (4.28),

$$\frac{\partial H_c(x^*)}{\partial x} = -\frac{\partial H(x^*)}{\partial x} = 0 \quad (4.40)$$

$$\frac{\partial^2 H_c(x^*)}{\partial^2 x} > -\frac{\partial^2 H(x^*)}{\partial^2 x} = 0 \quad (4.41)$$

Eqn.(4.40) indicates  $H_d$  has minimum value at equilibrium point  $x^*$ . and (4.41) indicates that  $x^*$  is the isolated stable point of the system. Thus, with the feedback controller (4.38), the closed-loop system is found asymptotically stable.

## 4.4 Load Torque Observer Design

In many cases, torque sensor for directly measuring load torque is not available. Thus, deriving its relations with current and speed is a practical method in solving unknown torque problem. When load of torque is constant, from (2.21) can get,

$$\dot{\omega}_r = \frac{3 \cdot N_p \cdot (L_d - L_q)}{2 \cdot J} \cdot i_d \cdot i_q + \frac{3 \cdot N_p \cdot \phi_m}{2 \cdot J} \cdot i_q - \frac{B_m}{J} \cdot \omega_r - \frac{\tau_L}{J} \quad (4.42)$$

$$\dot{\tau}_L = 0$$

Let the observation errors  $\tilde{\omega}_r = \omega_r - \hat{\omega}_r$  and  $\tilde{\tau}_L = \tau_L - \hat{\tau}_L$ , then one can construct load torque observer as,

$$\dot{\hat{\omega}}_r = \frac{3 \cdot N_p \cdot (L_d - L_q)}{2 \cdot J} \cdot i_d \cdot i_q + \frac{3 \cdot N_p \cdot \phi_m}{2 \cdot J} \cdot i_q - \frac{B_m}{J} \cdot \omega_r - \frac{\hat{\tau}_L}{J} + k_1 (\omega_r - \hat{\omega}_r) \quad (4.43)$$

A function of speed observer error as follows:

$$\dot{\hat{\tau}}_L = k_2 (\omega_r - \hat{\omega}_r) \quad (4.44)$$

where,  $k_1$  and  $k_2$  are designed observer gains,  $\hat{\omega}_r$  is the calculated speed from 4.43,

$\omega_r$ ,  $i_d$  and  $i_q$  are measured values.

$$\begin{aligned}\dot{\tilde{\omega}}_r &= \dot{\omega}_r - \dot{\hat{\omega}}_r = \left(-\frac{B_m}{J} - k_1\right)(\omega_r - \hat{\omega}_r) - \frac{1}{J}(\omega_r - \hat{\omega}_r) \\ \dot{\tilde{\tau}}_L &= \dot{\tau}_L - \dot{\hat{\tau}}_L = -k_2(\omega_r - \hat{\omega}_r)\end{aligned}\quad (4.45)$$

In matrix form (4.45) can be written as,

$$\begin{bmatrix} \dot{\tilde{\omega}}_r \\ \dot{\tilde{\tau}}_L \end{bmatrix} = \begin{bmatrix} -\frac{B_m}{J} - k_1 & -\frac{1}{J} \\ -k_2 & 0 \end{bmatrix} \cdot \begin{bmatrix} \tilde{\omega}_r \\ \tilde{\tau}_L \end{bmatrix}\quad (4.46)$$

Utilizing the pole placement method,

$$\begin{vmatrix} \lambda + \frac{B_m}{J} + k_1 & \frac{1}{J} \\ k_2 & \lambda \end{vmatrix} = \lambda^2 + \lambda \left(k_1 + \frac{B_m}{J}\right) - \frac{k_2}{J}\quad (4.47)$$

where  $\lambda$  is eigen values.

$$\lambda = \frac{-\left(k_1 + \frac{B_m}{J}\right) \pm \sqrt{\left(k_1 + \frac{B_m}{J}\right)^2 + \frac{4k_2}{J}}}{2}\quad (4.48)$$

Two poles are placed in  $-p$  ( $p > 0$ ) to stabilize the observer. Then, the relations for observer gains are obtained as,

$$\begin{aligned}-\left(k_1 + \frac{B_m}{J}\right) &= -p \\ \left(k_1 + \frac{B_m}{J}\right)^2 + \frac{4k_2}{J} &= 0\end{aligned}\quad (4.49)$$

Thus,  $k_1$  and  $k_2$  could be solved as,

$$\begin{aligned} k_1 &= 2p - \frac{B_m}{J} \\ k_2 &= -J \cdot p^2 \end{aligned} \tag{4.50}$$

An appropriate value of  $p$  could force the estimation error approaching to zero and compel the estimated torque  $\hat{\tau}_L$  converging to actual torque  $\tau_L$ . Thus, replacing  $\tau_L$  by estimated torque in the q-axis reference current section, the final control law for unknown torque scenario could be derived. To be noticed is that whether torque is given or not does not affect the original Hamiltonian structure of the system.

$$\begin{aligned} V_d &= -r_1(i_d - i_d^*) - J_{12}\left(i_q - \frac{2\hat{\tau}_L^* + 2B_m\omega_r^*}{3N_p\phi_m}\right) - J_{13}(\omega_r - \omega_r^*) + R_s i_d^* - N_p L_q i_q \omega_r^* \\ V_q &= J_{12}(i_d - i_d^*) - r_2\left(i_q - \frac{2\hat{\tau}_L^* + 2B_m\omega_r^*}{3N_p\phi_m}\right) - J_{23}(\omega_r - \omega_r^*) + R_s \cdot \frac{2\hat{\tau}_L^* + 2B_m\omega_r^*}{3N_p\phi_m} \\ &\quad + N_p L_d i_d \omega_r^* + N_p \phi_m \omega_r^* \end{aligned} \tag{4.51}$$

## 4.5 Conclusion

The design of IPMSM speed controller has been presented in the Chapter based on port controlled Hamiltonian with dissipation model. Firstly, based on dissipation inequality, introducing the concepts of dissipation and passive system. Then, the derivation of PCHD model from Euler-Lagrangian along with its stability proof was detailed in this section. The procedure of constructing an appropriate PCHD model, including the selection of correct state variables  $x_i$ , suitable interconnection matrix  $J(x)$  and damping matrix  $R(x)$ , adequate energy function  $H(x)$  and proper equilibrium point have also been provided. Theorem

(4.3) are the key factor of controller design. Final closed-loop model and control law are established based on its results. Due to the particular requirement (lacking of torque sensor) for real-time experiment, a torque observer is also needed for accurate operation. The last section discussed the estimation of load torque based on detectable variatals. By utilizing pole placement method, the designed torque observer tracking capability with torque variation rapidly and precisely was guaranteed. Final step was replacing the unknown parameters with estimated one in the context of remaining the PCHD structure unaltered.

# Chapter 5

## System Simulation

### 5.1 Introduction

The performance of the  $H_\infty$  controller and nonlinear PCHD controller are investigated in simulation using Matlab/Simulink environment to predict the behaviour of the system before the real time implementation.

The overall IPMSM speed control system shown in Fig.5.1 is built in Matlab/Simulink software based on mathematical models for each component. In Fig.5.1, PWM signal is expressed based on if/else logic comparison statements, inverter model is carried out by a scaled summation of three phase PWM signals overtime. In addition, same as the “speed reference”, “load” is directly given out by a varied signal, and the block “IPMSM” is established according to (2.21). Each block is detailed in Fig.B.1 to Fig.B.6.

The performance of proposed speed controller is investigated under diverse set of operating conditions. Such as ramp and step changes of reference signal, external load disturbances, parameter variations etc. Horizontal comparisons are made between conventional tuned PI controller, mixed-sensitivity based  $H_\infty$  controller

and nonlinear PCHD controller in order to demonstrate the improvements of the proposed controller. Uncertainty attenuation abilities for  $H_\infty$  controllers are verified and shown by longitudinal comparisons.

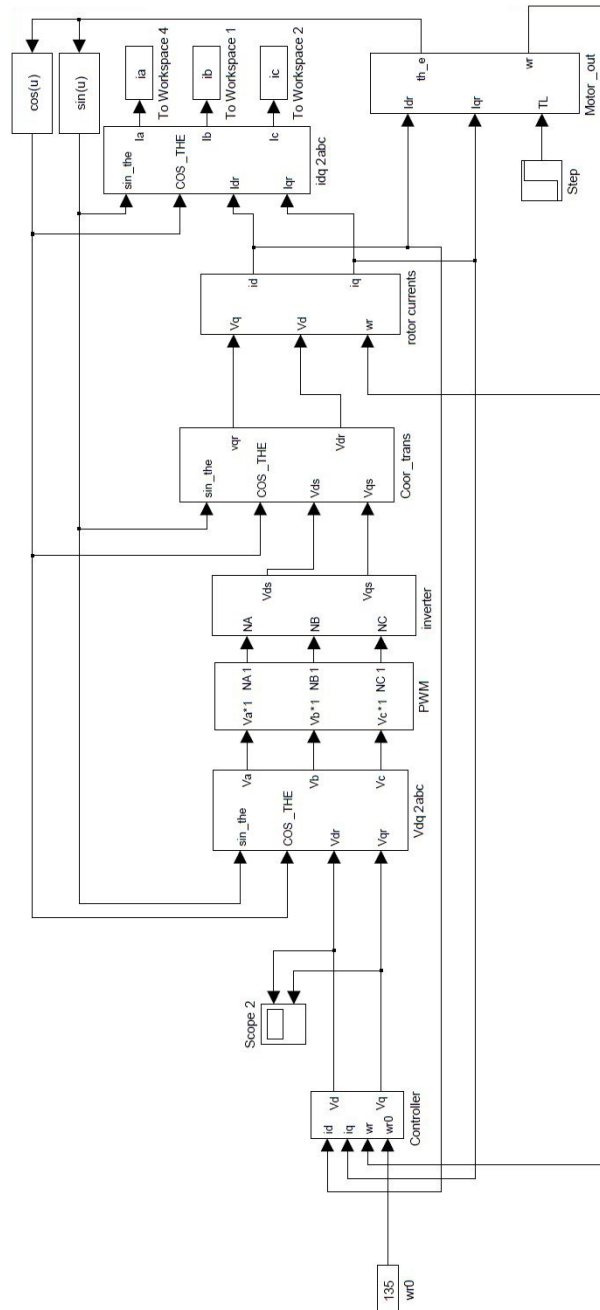


Figure 5.1: IPMSM speed control system schematic in Simulink software.

## 5.2 Simulation Results

The parameters and coefficients of IPMSM utilized in this simulation are listed in Appendix-A. Sampling time for solving differential equations are fixed at 0.0001 s in simulation considering future real-time experiment.

For comparative propose, conventional tuned PI controller is also designed and simulated. In order to achieve quick response, small overshoot and accurate tracking speed, based on online trial and error approach, the proportional gain and integral gain for speed PI controller are chosen as 1.5 and 8, for d-axis current PI controller are set as 25 and 50, for q-axis current PI controller gains are selected as 1.5 and 75.

$H_\infty$  controller in this thesis utilizes Robust Control Toolbox in Matlab to compute desired controllers. As the controller is precalculated and cannot be tuned during the ongoing simulation process, weight function of proposed  $H_\infty$  controller is tuned off-line based on trail and error to get the optimum performance. For simulation, weight functions are selected as follows:

$$W_1 = \frac{5 \cdot s + 1000}{10 \cdot s + 0.1} \quad W_2 = 0.08 \quad W_3 = \frac{0.5 \cdot s + 50}{0.1 \cdot s + 1000}$$

Gains for non-linear PCHD controller are chosen as 5, 10, 2, 3, 10 for  $r_1$ ,  $r_2$ ,  $J_{12}$ ,  $J_{13}$  and  $J_{23}$  respectively. To ensure tracking ability of torque observer, coefficient “ $p$ ” is selected as  $-500$ .

### 5.2.1 Simulation Results of $H_\infty$ Controller

Frequency characteristics of sensitivity function and complementary sensitivity function are shown in Fig.5.2(a) and Fig.5.2(b) , which meet expectations in 3.22 and 3.24, respectively.

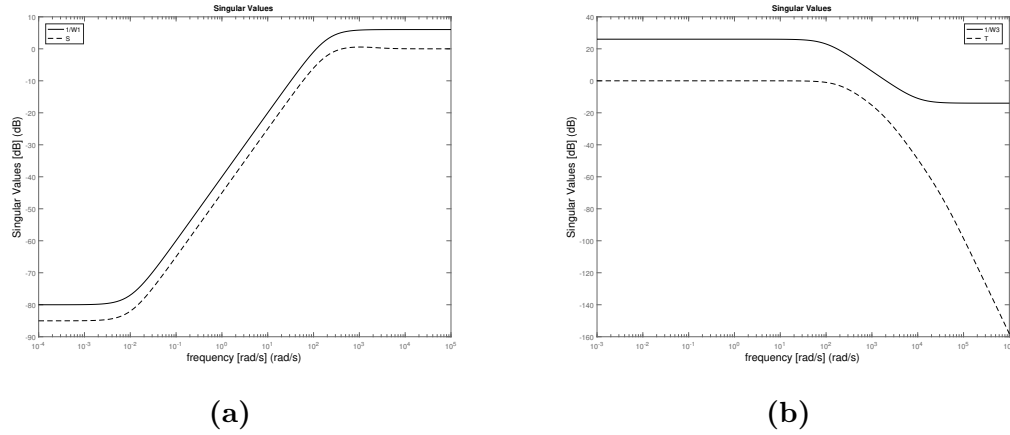


**Figure 5.2:** Frequency characteristics of sensitivity function and complementary sensitivity function: (a)sensitivity function (b)complementary sensitivity function

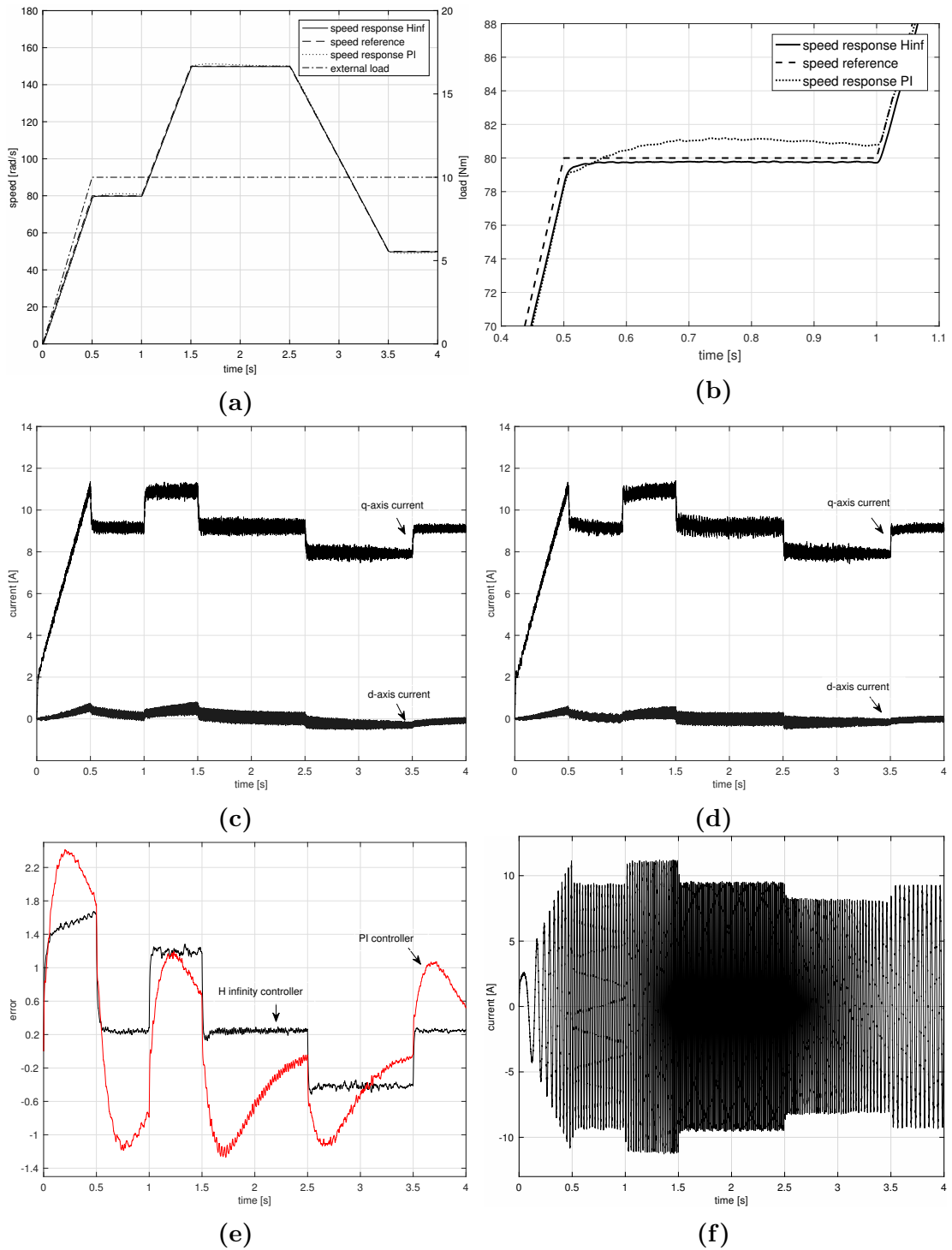
Fig.5.3 shows the simulation results of the proposed  $H_\infty$  controller for ramp speed reference signal with increased load to 50% rated load ( $10 N \cdot m$ ) over a  $500 ms$  interval. The reference speed signal is increased to  $80 rad/s$  at  $500 ms$  and then start rising to  $150 rad/s$  from  $1 s$  to  $1.5 s$ . Then it is started to decrease to  $50 rad/s$  at  $t = 2.5 s$  in  $1 s$ . The performance results of the proposed  $H_\infty$  controller is compared with the conventional tuned PI controller for improvement investigation.

Fig.5.3(a) shows the speed response of the proposed  $H_\infty$  controller utilizing mixed-sensitivity controller in left axis, with the actual external torque applied in the right axis. For clarity, a zoom in view of the speed response in Fig.5.3(a) is shown in Fig.5.3(b). It is found that the tracking performance of the proposed  $H_\infty$  controller is superior to the conventional tuned PI controller in terms of steady-state error. D-q axis currents responses are shown in Fig.5.3(c) and Fig.5.3(d) separately in order to avoid overlaps.  $H_\infty$  controller demonstrate less current ripple and spikes than that of PI controller. Fig.5.3(e) shows the speed error dynamics, due to the change of reference speed, speed error is slightly larger than that of in

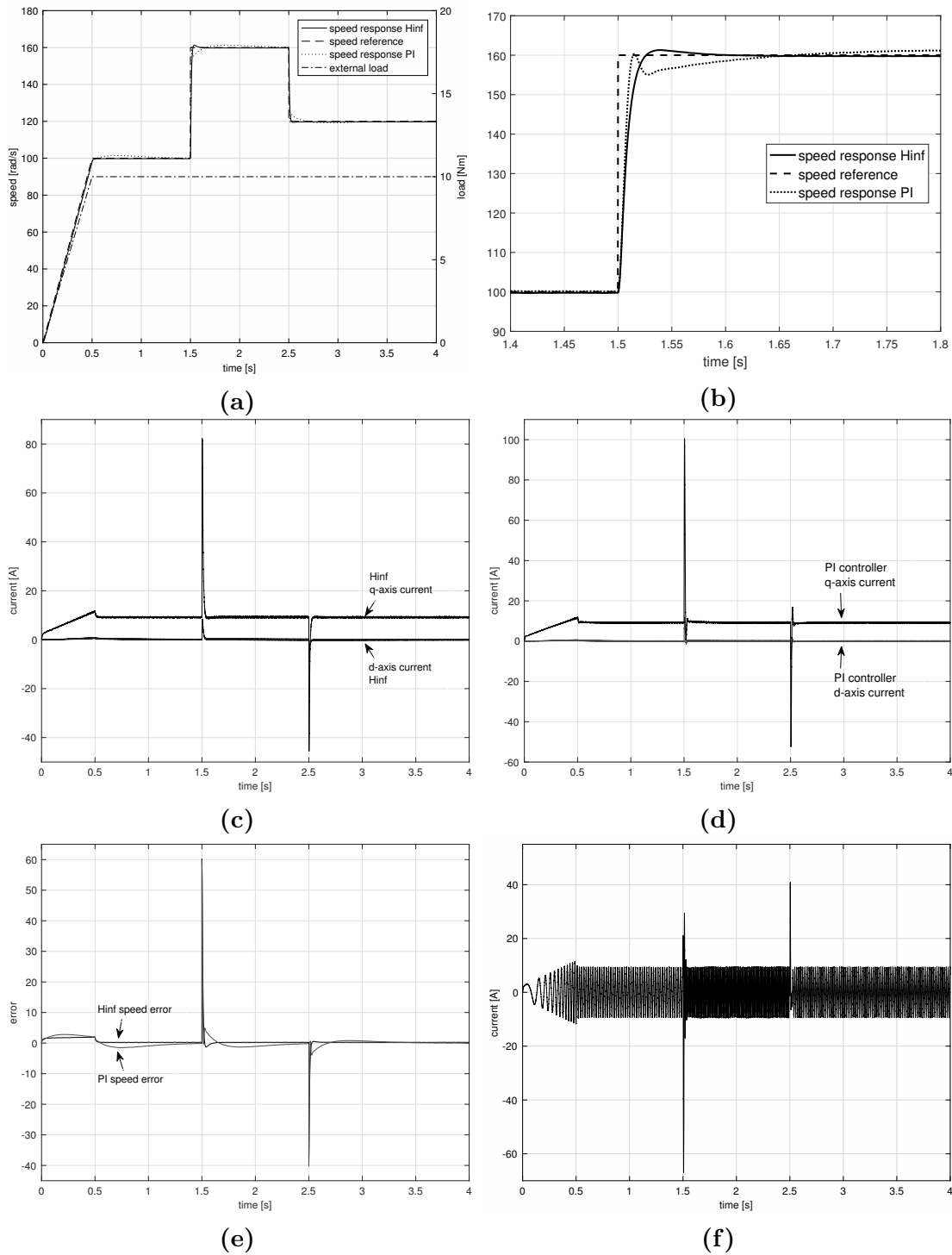
steady state. A tiny offset error about  $0.2 \text{ rad/s}$  are observable for the proposed  $H_\infty$  controller which is in the range of acceptable limit while PI controller shows slower tracking ability and larger steady state offset. Fig.5.3(f) indicates that the phase current is within the maximum permissible value.

Fig.5.4 shows the response of the proposed  $H_\infty$  controller for a step change in speed reference signal. At the starting moment ramp speed reference signal ( $0\text{-}100 \text{ rad/s}$ ) is applied to avoid any stator current surge. Then at  $t = 1.5\text{s}$ , step increase in speed reference from  $100 \text{ rad/s}$  to  $160 \text{ rad/s}$  and at  $t = 2.5\text{s}$ , a step decrease in speed reference from  $160 \text{ rad/s}$  to  $120 \text{ rad/s}$  is applied. The performance of the proposed  $H_\infty$  controller is also compared with the conventional tuned PI controller.

Compared with conventional tuned PI controller in Fig.5.4(a) and its zoom in view Fig.5.4(b), it is found that proposed  $H_\infty$  controller has less steady-state error and quicker converge ability than that of conventional tuned PI controller. Compared Fig.5.3(c) and Fig.5.4(d), it is noticed that current spike is naturally exist in both type of controllers but proposed  $H_\infty$  controller has smaller spikes which prevent in damaging equipment. Fig.5.4(e) demonstrates the speed error dynamics, it is clearly perform less steady-state error and quicker converge speed that the proposed  $H_\infty$  controller has. In real-time experiment, current spikes would be smaller because of the limitation of power supply and applied load. Despite the proposed  $H_\infty$  controller has small overshoot (1.25%) when applying a step signal, tracking ability is fast and accurate.



**Figure 5.3:** Responses of the proposed  $H_\infty$  controller for a ramp speed reference signal: (a) speed response overview (b) zoom in view from 0.5 to 1 s (c) d-q axis currents response (d) d-q axis currents response of PI controller (e) speed error comparison (f) single phase current of  $H_\infty$  controller.



**Figure 5.4:** Response of the proposed  $H_\infty$  controller for step changes speed reference signal from 100 – 160 – 120 rad/s (a) speed response overview (b) zoom in view from 1.5 to 2 s (c) d-q axis currents response of  $H_\infty$  controller (d) d-q axis currents response of PI controller (e) speed error comparison (f) single phase current of  $H_\infty$  controller

A series of load changes is also applied for  $H_\infty$  controller to demonstrate its performance on disturbance attenuation ability. Load variation is changed in slope to prevent destabilization. With the reference speed given at  $160 \text{ rad/s}$ , the external load is changed from 0 to its 50% rated from 0 to  $0.3 \text{ s}$ , from  $0.3 \text{ s}$  to  $1 \text{ s}$ , load remains constant at  $10 \text{ N} \cdot \text{m}$  and then the load is increased to full load ( $20 \text{ N} \cdot \text{m}$ ) from  $1 \text{ s}$  to  $1.5 \text{ s}$ . Again the load is decreased from  $20 \text{ N} \cdot \text{m}$  to  $5 \text{ N} \cdot \text{m}$  from  $2.5 \text{ s}$  to  $3 \text{ s}$ , after that the load remain constant at  $5 \text{ N} \cdot \text{m}$ . It is clearly seen from Fig.5.5(a) the proposed  $H_\infty$  controller shows an excellent ability to rapidly converge to the reference signal after each load disturbance applied than that of the conventional tuned PI controller. The corresponding speed tracking errors are shown in Fig.5.5(b), which shows the lower speed error for  $H_\infty$  controller than that of PI controller which further verifies the earlier speed response. However, the d-q axis current control is still using PI controller and consequently, the d-q axis current responses do not show huge improvement as the speed response. That is the reason the nonlinear PCHD controller was developed and its performance is tested in the next section.

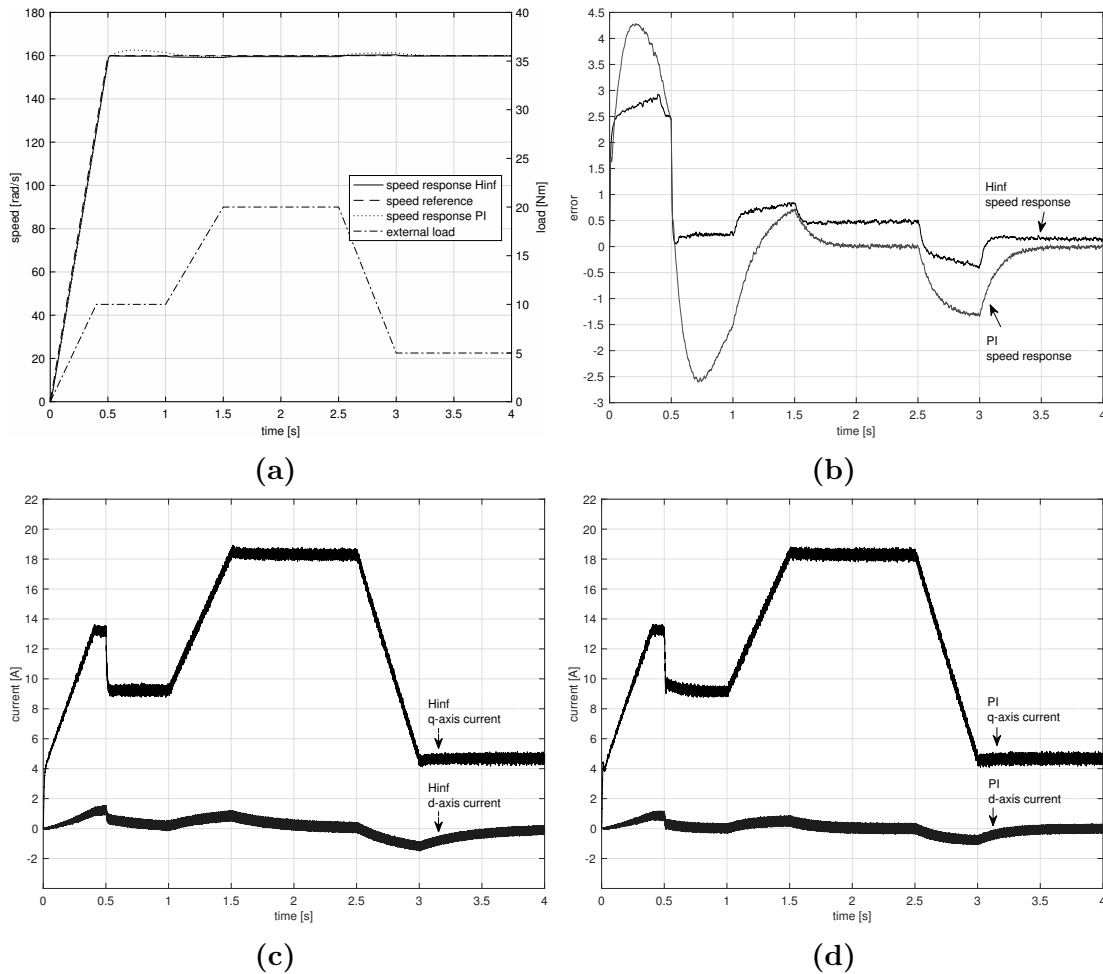


**Figure 5.5:** Performance of the proposed  $H_\infty$  based IPMSM drive for ramp changes in external load: (a) comparative speed responses (b) speed error comparison (c) d-q axis currents response of  $H_\infty$  controller (d) d-q axis currents response of PI controller

During the motor's operation, it is impossible that the parameters will remain at nominal value all the time, such as temperatures has great influence on stator resistance, q axis inductance may alter because of flux saturation and stator current. Fig.5.6 shows the speed and current responses of the proposed  $H_\infty$  controller with different parameters besides nominal values but at the same speed and load conditions indicated in Fig.5.4. And focus is on the first step change in reference speed at  $t = 1s$ . It clearly shows that in scenarios like stator resistance tripled, q-axis inductance doubled or become half of the original value,  $H_\infty$  controller can

still be reliable. Only the overshoot changes during transient condition. Thus,  $H_\infty$  controller demonstrate the ability to handle uncertainty. Fig.5.7 shows the balanced three phase current at rated load condition.

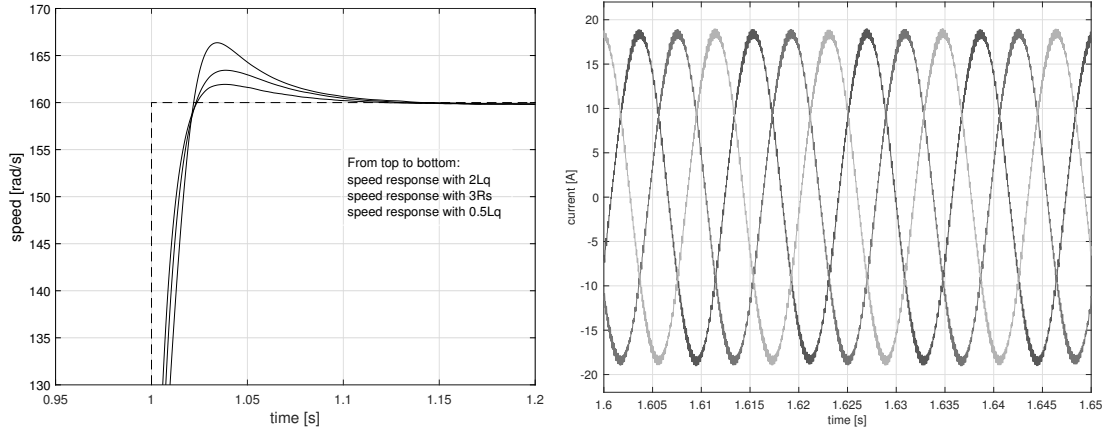


**Figure 5.6:** Performance of the proposed  $H_\infty$  controller with parameter variations.

**Figure 5.7:** Balanced three phased currents for  $H_\infty$  controller.

### 5.2.2 Simulation Results of PCHD Controller

This section demonstrate the simulation results of earlier developed nonlinear PCHD controller. Fig.5.8 shows the system performance of the proposed nonlinear PCHD controller based IPMSM drive for ramp speed reference signal with the 50% rated load. Both speed and load reference signal are applied same as in Fig.5.3.

Fig.5.8(a) demonstrates the speed response of proposed nonlinear PCHD controller could closely follow the command signal. With the speed error dynamics showed in Fig.5.8(b), it is found that PCHD controller shows a better performance than that of conventional tuned PI controller in speed tracking ability and steady-state error attenuation ability. Speed error of proposed PCHD controller can converge to almost zero at steady speed with a little offset while PI controller experienced huge overshoot and steady error. D-q axis current response of PCHD controller is shown in Fig.5.8(c) which has the same performance as that of PI

controller.

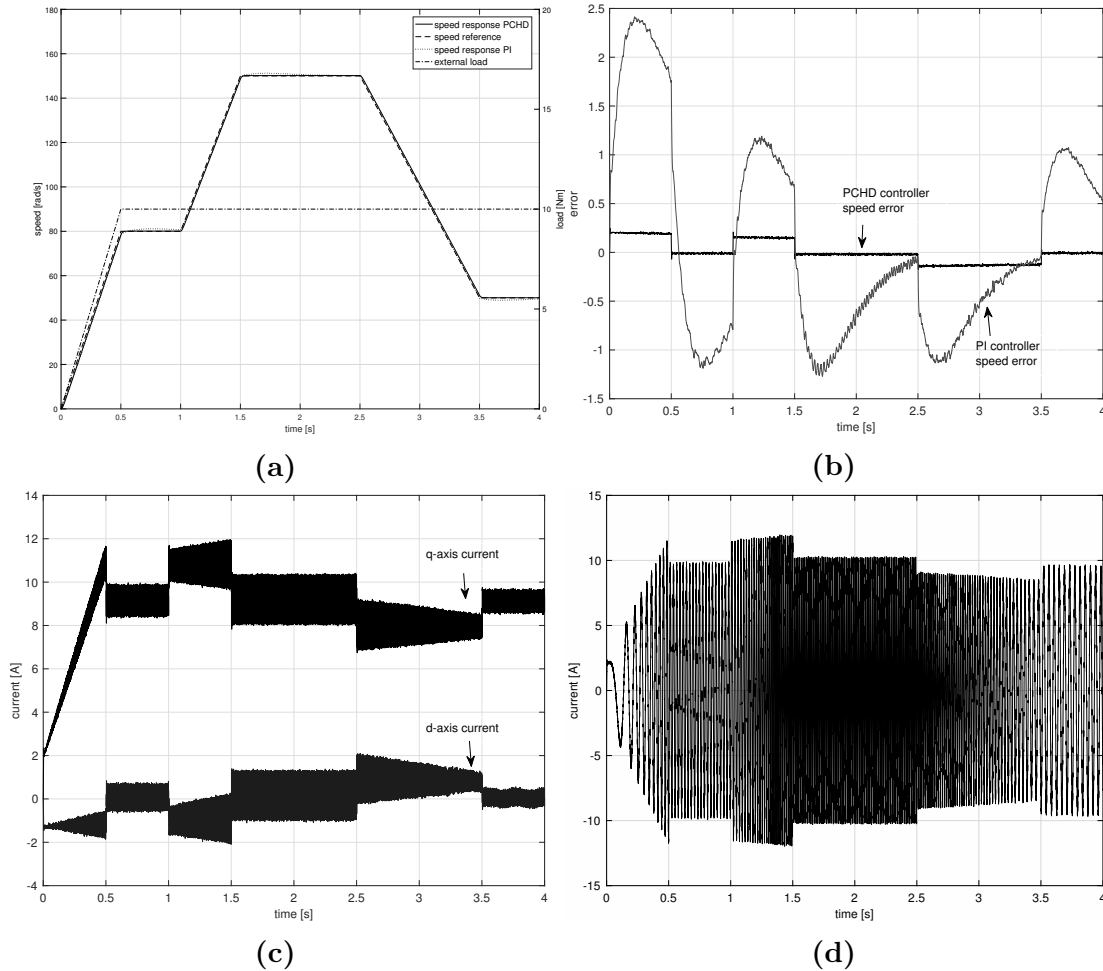


**Figure 5.8:** Response of the proposed nonlinear PCHD controller for a ramp reference signal: (a) speed response overview (b) speed error comparison with conventional tuned PI controller (c) d-q axis currents response (d) single phase current of PCHD controller.

Fig.5.9 shows the response of proposed nonlinear PCHD controller for a step change in speed reference signal. The speed and load reference signals are applied same as in Fig.5.4. The performance of the proposed PCHD controller is compared with previous  $H_\infty$  controller and conventional tuned PI controller. It is clearly seen from Fig.5.9(a) and Fig.5.9(b) that proposed PCHD controller shows the ability of tracking reference speed signal rapidly with tiny offset. As the d-q axis current response shown in Fig.5.9(c), proposed nonlinear PCHD controller demonstrates

smaller current spikes when step signal is applied at  $t = 1.5s$  and  $t = 2.5s$  than that of  $H_\infty$  controller and PI controller in Fig.5.4(c) and Fig.5.4(d), respectively.

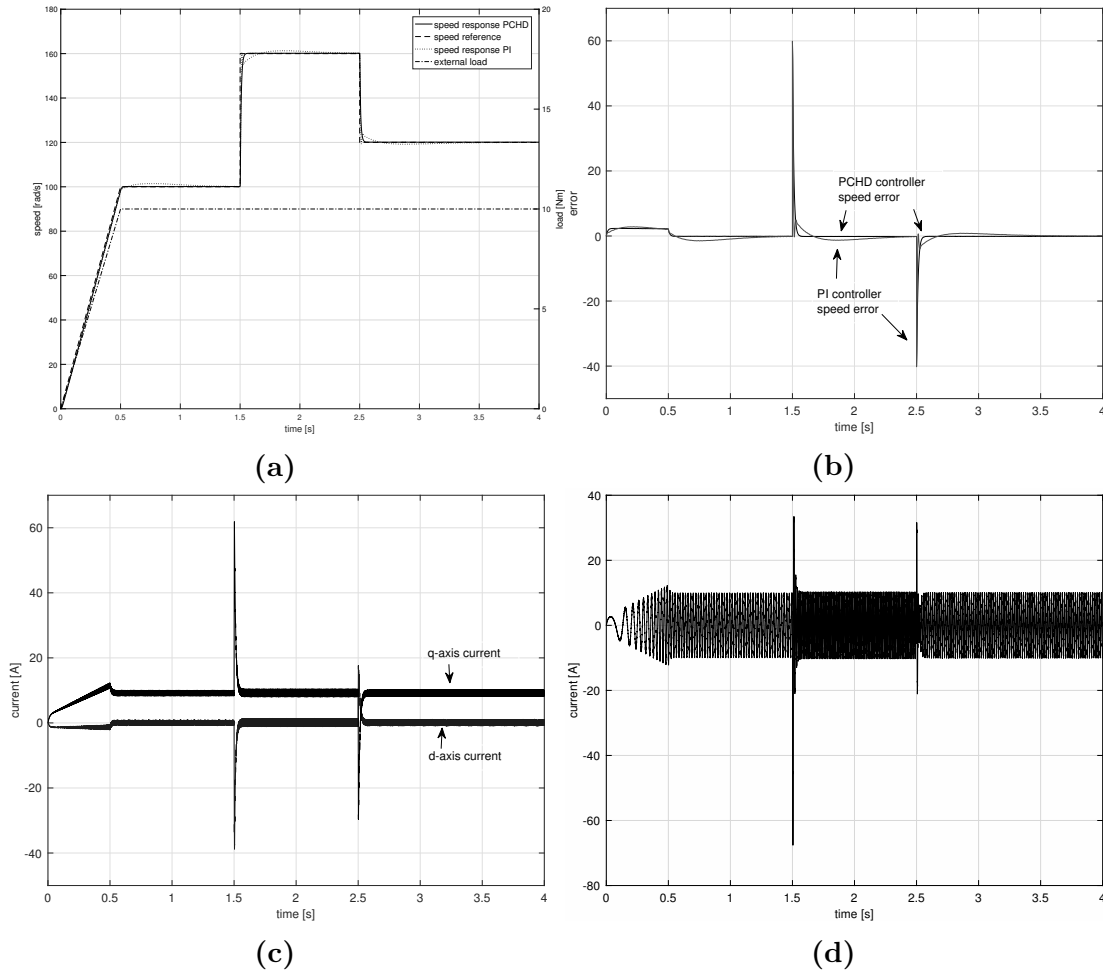


**Figure 5.9:** Response of the proposed nonlinear PCHD controller for step changes reference speed signal: (a) speed response overview (b) speed error comparison (c) d-q axis currents response (d) single phase current response.

The performance of the proposed nonlinear PCHD controller is also investigated by applying a series of load changes in Fig.5.10. Load variation signal and speed reference signal are applied as the same as in Fig.5.5. Fig.5.10(a) and Fig.5.10(b) demonstrate speed response and error dynamic of proposed PCHD controller. They clearly show the speed response does not affected too much by load changing. In addition, motor speed can instantly recover to the command speed

level once external load in steady. On the contrary, PI controller required more time to stabilize the motor speed. , d-q axis current is shown in Fig.5.10(c) to demonstrate proposed nonlinear PCHD controller has less spikes than that of PI controller. Likewise, phase current in Fig.5.8(d), Fig.5.9(d) and Fig.5.10(d) are maintained in the range of maximum limitation.

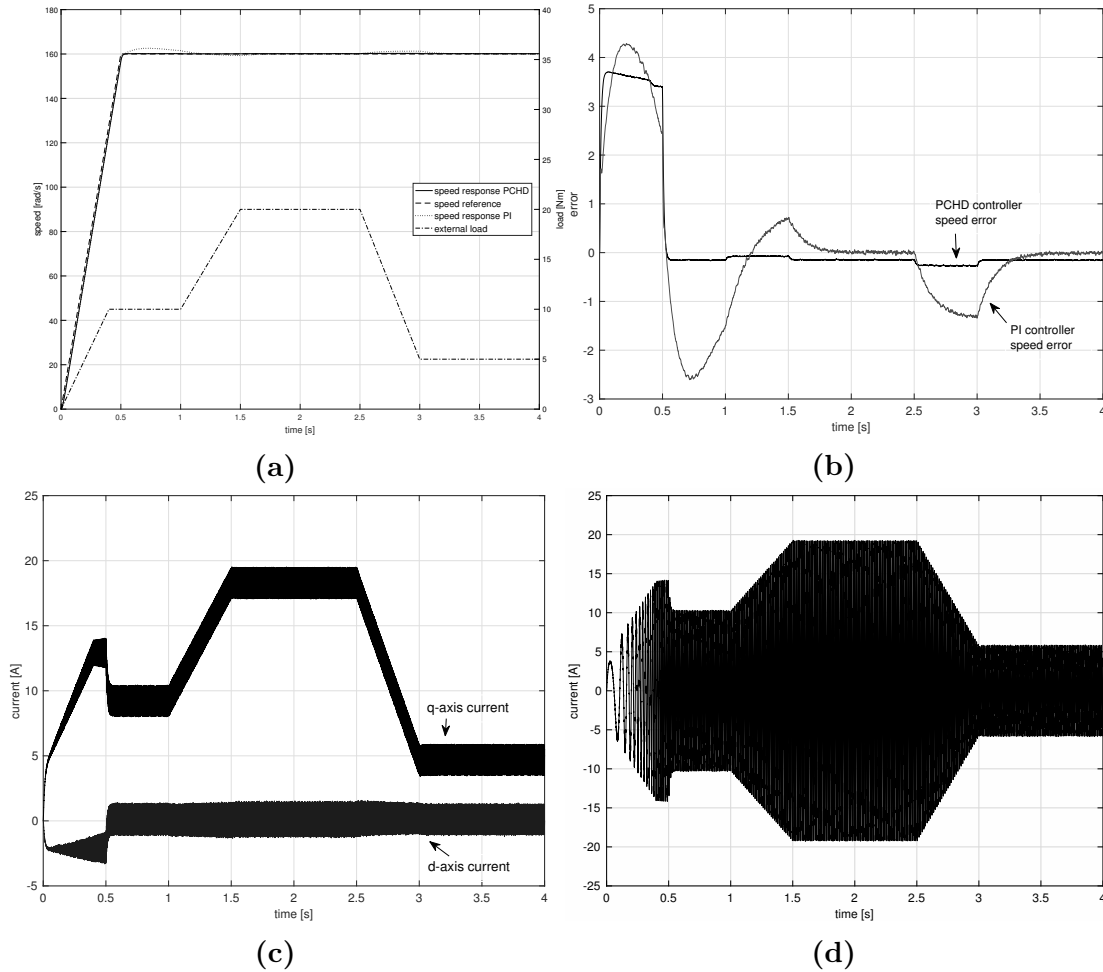


**Figure 5.10:** Performance of the proposed nonlinear PCHD controller based IPMSM drive for ramp changes in external load: (a) comparative speed response (b) speed error dynamic comparison (c) d-q axis currents response (d) single phase current response

Speed reference signal changes in ramp and step plus load reference signal variation tested the PCHD controller is a reliable nonlinear controller under complex operating conditions. It can closely follow the speed command signal

whether it's a ramp or a step signal and it can also keep tracking desired speed when external load suddenly altered.

Due to the limitation of real-time setup in this thesis, load sensor is absent. Thus, calculations from known variables and parameters to estimate actual torque is required, as shown in Equ.(4.43). Fig.5.11 demonstrates the torque observer error dynamics for conditions shown in Fig.5.8, Fig.5.9 and Fig.5.10. With the maximum error is maintained at 0.27, torque observer designed in (4.43) demonstrates a reliable performance.

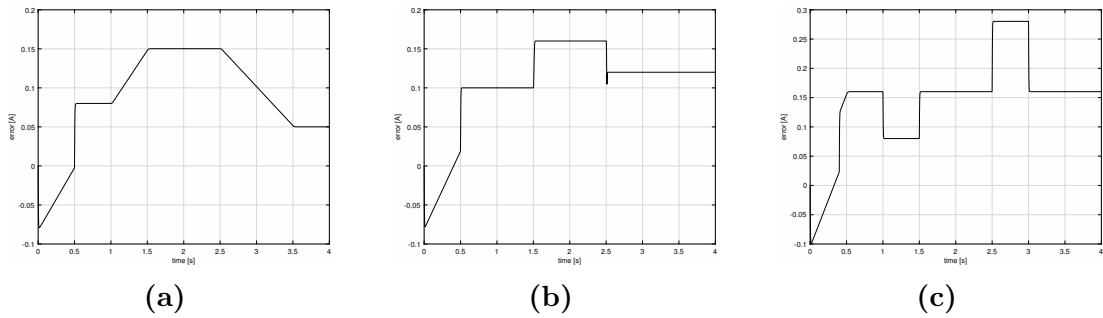


**Figure 5.11:** Error dynamics of proposed torque observer (a) ramp speed reference signal (b) step speed reference signal (c) external load variation signal

## 5.3 Conclusion

The performance of the proposed  $H_\infty$  and PCHD controller based IPMSM drive have been investigated extensively in simulation at different operating conditions, such as changes changes in reference speed, external load and parameters. Both  $H_\infty$  and PCHD controllers demonstrated excellent performance as compared to conventional tuned PI controller. However, it was found that PCHD exhibited better performance than that of  $H_\infty$  controller in the context of less steady-state error.

# Chapter 6

## Real Time Implementation

Simulation results presented in previous chapter encouraged to implement the developed control algorithms in real-time. The detail real-time implementation procedure of the proposed  $H_\infty$  and PCHD controllers based IPMSM drive is presented in this chapter. For real-time implementation dSPACE digital signal processor (DSP) controller based DS1104 is used in this work. The DSP computes 6 pulse width modulation (PWM) signals based on the control algorithm and operates inverter in order to drive the target motor. Feedback signals (motor position and d-q axis current) detected by existing sensors are sent back to DSP for computation in the next step.

### 6.1 Hardware Overview

The DSP DS1104 board is installed on an Intel based PC and communicate via peripheral component interface (PCI) bus. ControlDesk real time interface (RTI) is responsible for sending command variables to DS1104 and receiving monitoring signals in real time. This enable users to establish customized graphical interfaces

and tuning control parameters during the motor operation. As per Fig.6.1, master processor of DS1104 board is MPC8240, which is a 64bit floating point processor with clock speed at 250MHZ and dual slot 16KB cache. The loaded control algorithm will be running on master processor. Slave processor is which used for generate PWM signals is based on TMS320F240, a 16bit fixed point processor made by Texas Instruments (TI). Hall effect based linear current sensors (ACS758x050B) is used for motor current measurement and signals are fed to A/D converter after amplified to 5V level. Due to the ungrounded neutral point of motor, only two phase currents are measured and third phase is calculated based on balanced three phase relations. The motor speed is computed from motor position sensor using numerical differentiation, which is mounted on the one end of motor shaft and the signal is transferred to DSP board by incremental encoder interface (CP19), as shown in Fig.6.3. An NTE7407 hex buffer is used for boosting PWM signals to proper voltage levels in order to reach the threshold voltage of IGBTs. And D/A channels giving out desired real-time experimented results to Tektronix TPS2024 oscilloscope.

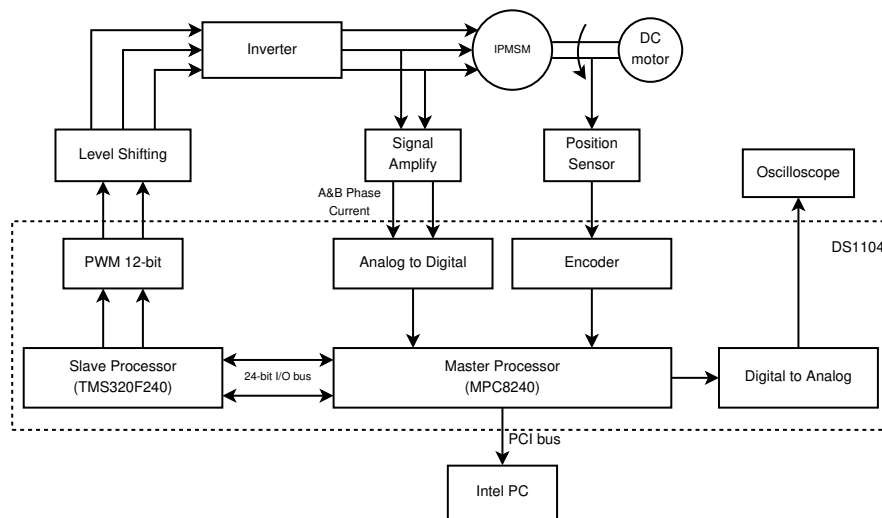


**Figure 6.1:** Block diagram of real-time hardware setup of experimental system based on DS1104 board.

Each major equipment utilized in this experiment is detailed in the following. Those specifications and ratings are given in Table.6.1. And a picture of experimental set up environment is shown in Fig.6.2 with labelled major components for reference.

**Table 6.1:** System specifications and ratings

Component	Manufacturer	Model	Specification
Controller Board	dSPACE GmbH	DS1104	Clock Frequency $250MHz$ ADC/DAC 16-bit Encoder 10-bit PWM 12-bit
Inverter	Semikron	AN-8005	DC supply $< 750V$ Phase current $< 30A$ Drive input $0/15V$
IPMSM motor	Yaskawa	686SS	refer to Table.A.1
Current sensor	Allegro	ACS758x050B	Current rating $\pm 50V$
Position sensor	Sumtak	LMA-102	Resolution 10-bit
Power Supply (AC transformer)			Voltage up to $600V$

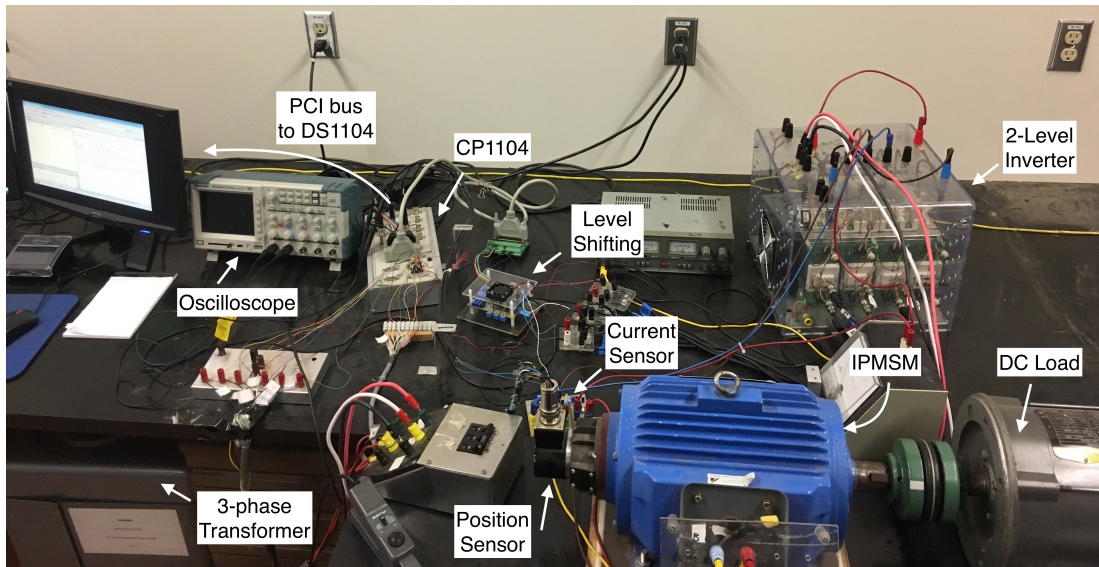


**Figure 6.2:** Experimental setup environment for the complete IPMSM drive.

All connections on the DS1104 board are reachable through CP1104 connection panel which is referenced in Fig.6.3. Where BNC connectors CP1 to CP8 are A/D channels, CP9 to CP16 used as D/A channels.

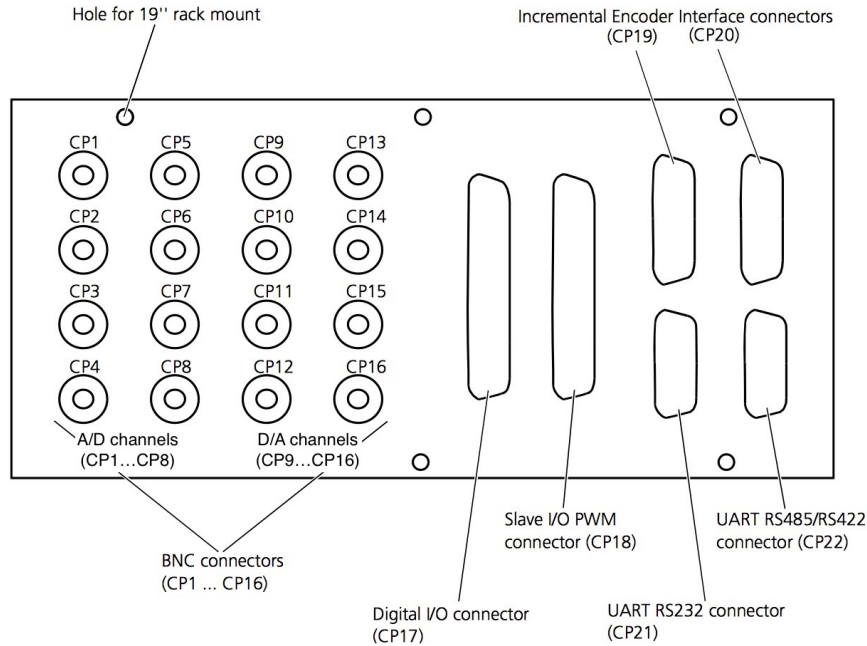


**Figure 6.3:** CP1104 connection panel

The control algorithm is firstly constructed in real-time Simulink using regular MATLAB computational mathematical features with I/O communication modules form “rtlib1104” library. And then real-time files “.mdl” or “.slx” (depend on MATLAB/Simulink version) are compiled into C language by Simulink software. Executable files with “.ppc” and “.obj” extensions are created during the compilation process, and loaded on master and slave processors, respectively. The compiler is installed in parallel with dSPACE software, thus the ControlDesk can detect and run the loaded code. After several times of trail and error, to ensure the DSP board can process the algorithm within each sampling time, the sampling rate is fixed at  $100\mu s$  in this thesis. Smaller sampling rate is possible unless with more powerful DSP board and reduced complexity of control algorithms.

The inverter is supplied from an uncontrolled rectifier fed by a variable AC transformer, capable of supplying up to 600V through an uncontrolled rectifier. Dynamic load to the motor is provided by a DC generator, with variable resistive load connected to the stator.

## 6.2 Experimental Results

The effectiveness of the proposed  $H_\infty$  controller and nonlinear PCHD controller is verified by real-time experimental work in this section. Results are broken into three parts. Firstly, the dynamic performance under no load condition is presented, then followed by another comparison with 25% of load and finally, the steady state performance with 50% load at 70 rad/s were presented. Table 6.2 shows gains and parameters that used in real-time environment.

**Table 6.2:** Controllers parameter and gains

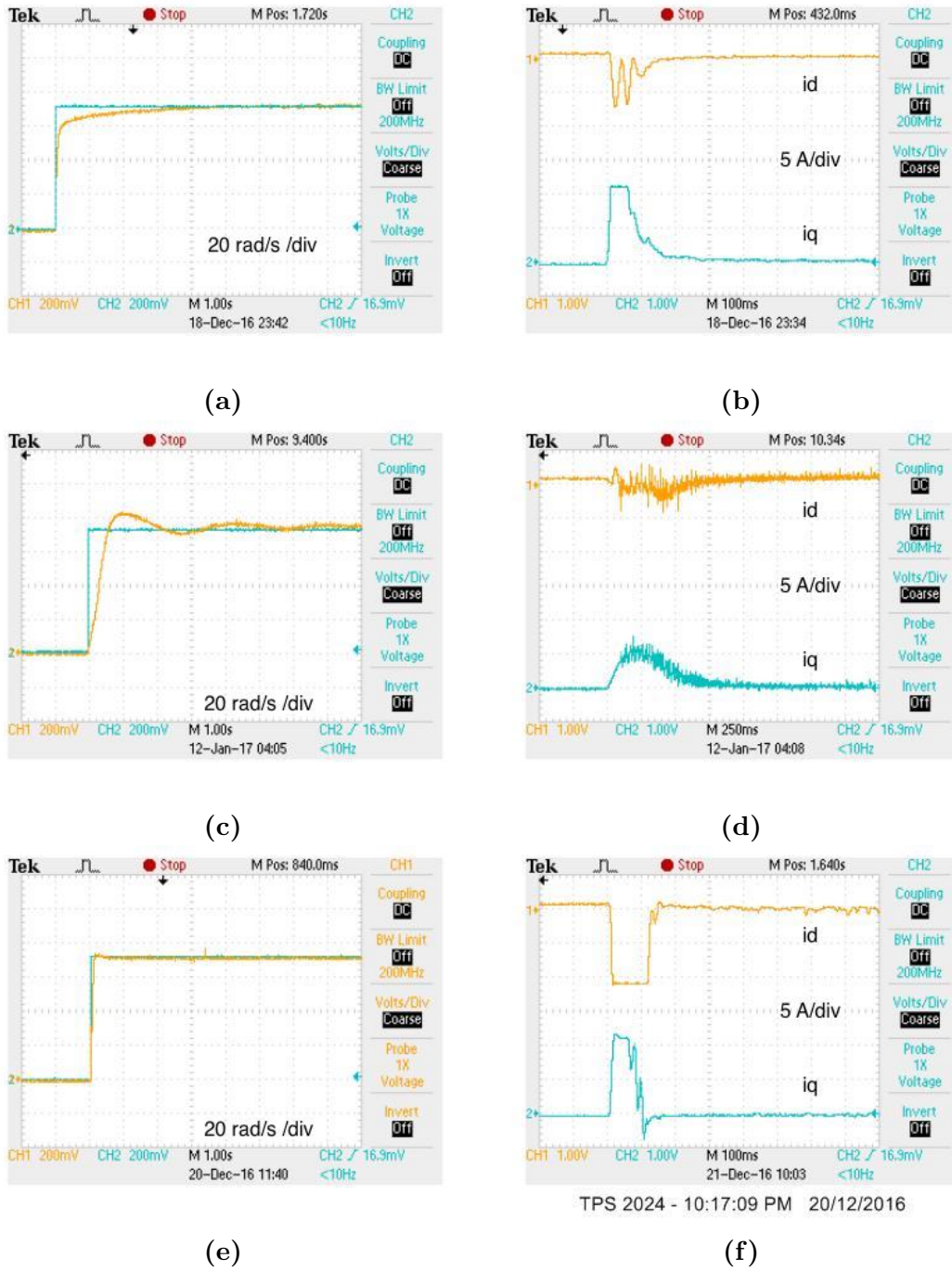
PI controller gains	d-axis P: 3	q-axis P: 4.5	speed P: 2
	d-axis I: 0.7	q-axis I: 7	speed I: 1.2
$H_\infty$ weight functions	$W_1 = \frac{80 * s + 1000}{10 * s + 0.1}$	$W_2 = 1$	$W_3 = \frac{0.5 * s + 600}{3 * s + 10000}$
PCHD controller gains	$J_{12} = 7$	$J_{13} = 5$	$J_{23} = 10$
	$r_1 = 3$	$r_2 = 15$	

Fig.6.4 shows the comparative real-time performance of the proposed  $H_\infty$  controller and nonlinear PCHD controller with tuned PI controller for step change in reference speed (from 0 to 70rad/s) at no load condition. Fig.6.4(a) and Fig.6.4(b) show the mechanical angular velocity and d-q axis current response of the conventional tuned PI controller, while the Fig.6.4(c), Fig.6.4(d) shows the results for  $H_\infty$  controller and Fig.6.4(e), Fig.6.4(f) for proposed PCHD nonlinear controller, respectively. It is found that the speed response for  $H_\infty$  controller is

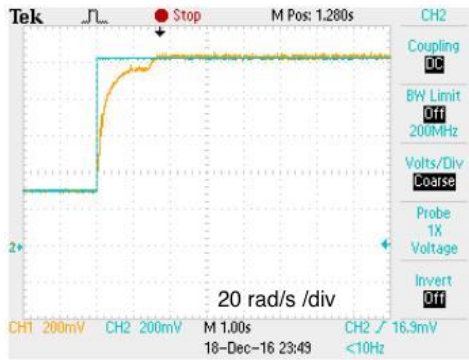
faster than that of PI controller but it suffers from overshoot and undershoot. However, the PCHD based nonlinear controller exhibits fastest speed response without any overshoot or undershoot.

The reason behind this phenomenon is that  $H_\infty$  controller is designed for the system's worst case scenario e.g., huge external load disturbance. On the contrary, PCHD nonlinear controller shows the ability to rapidly converge to command speed within less than 0.5s. In the d-q axis current response,  $H_\infty$  controller in Fig.6.4(d) demonstrates less spikes than other controllers. And Fig.6.4(f) clearly expresses the contribution of the d axis current in nonlinear PCHD controller during the speed change. The flat hat in Fig.6.4(b) and Fig.6.4(f) are due to current saturation, which is set at 22A to protect components.

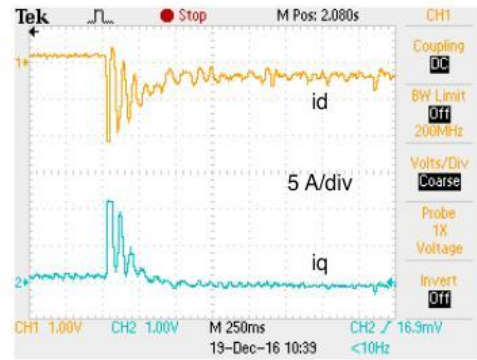
Fig.6.5 shows the performance of IPMSM drive for different controllers for step change in speed change from 30-100rad/s with 25% load. It is seen from Fig.6.5(a) that the conventional tuned PI controller takes 1.7s to converge to the command speed. Compared with  $H_\infty$  controller in Fig.6.5(c), speed response curve is not only has quicker setting time (less than 1s), but also smoother than that of conventional PI controller. Nonlinear PCHD controller in Fig.6.5(e) demonstrates the fastest speed response. Both  $H_\infty$  controller and PCHD controller have tolerable overshoot and speed ripple. D-q axis current responses show similar results as no load condition.  $H_\infty$  controller has less current spikes but more obvious current ripple, and PCHD demonstrate more contribution from d-axis current that causes the quickest speed response.



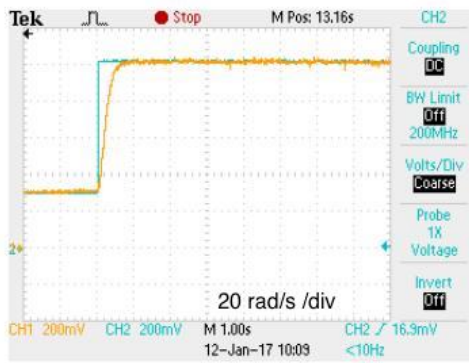
**Figure 6.4:** Experimental starting performance of the IPMSM drive: (a) speed response for conventional tuned PI controller (b) d-q axis current response for conventional tuned PI controller (c) speed response for proposed  $H_\infty$  controller with mixed-sensitivity approach (d) d-q axis current response for proposed  $H_\infty$  controller (e) speed response for proposed nonlinear PCHD controller (f) d-q axis current response for proposed nonlinear PCHD controller.



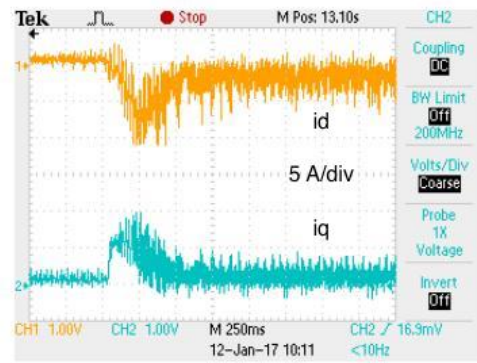
(a)



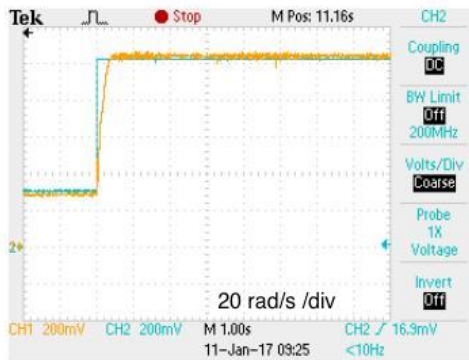
(b)



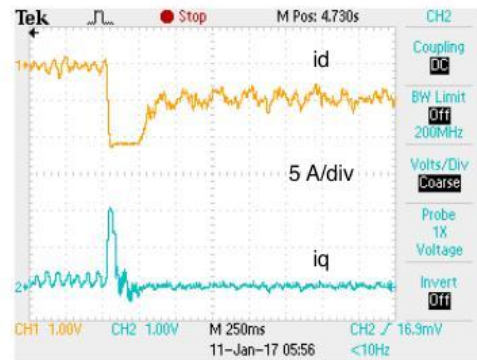
(c)



(d)

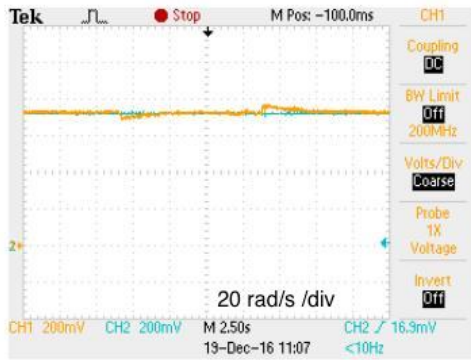


(e)

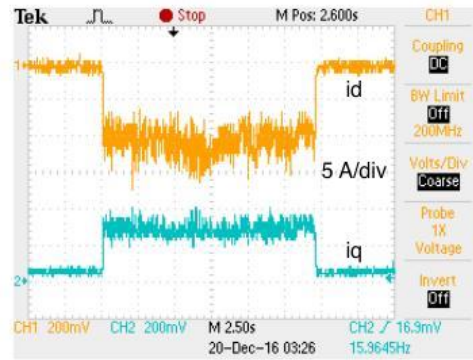


(f)

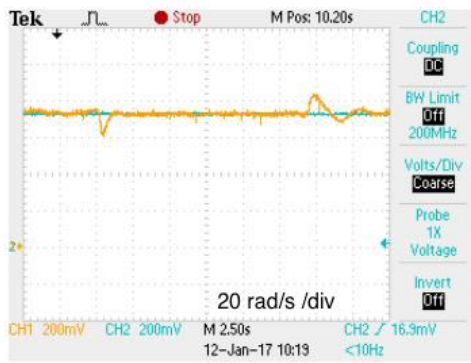
**Figure 6.5:** Experimental performance of IPMSM drive with various controller for step changes in command speed  $30\text{-}100\text{rad/s}$  with 25% rated load (a) speed response for conventional tuned PI controller (b) d-q axis current response for conventional tuned PI controller (c) speed response for  $H_\infty$  controller (d) d-q axis current response for  $H_\infty$  controller (e) speed response for nonlinear PCHD controller (f) d-q axis current response nonlinear PCHD controller.



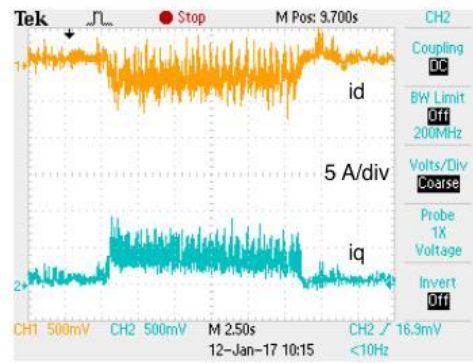
(a)



(b)



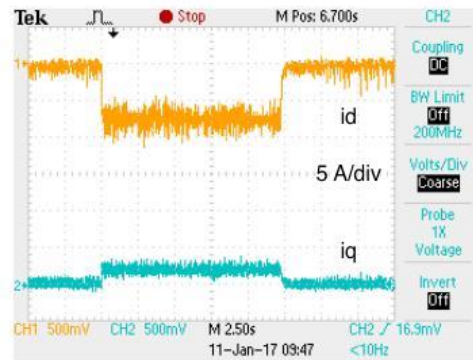
(c)



(d)



(e)



(f)

**Figure 6.6:** Experimental performance of IPMSM drive with various controller for steady command speed in  $70\text{rad/s}$  with 50% rated load (a) speed response for conventional tuned PI controller (b) d-q axis current response for conventional tuned PI controller (c) speed response for  $H_\infty$  controller (d) d-q axis current response for  $H_\infty$  controller (e) speed response for nonlinear PCHD controller (f) d-q axis current response nonlinear PCHD controller.

Fig.6.6 shows the performance of the proposed controllers for step changes in load at a fixed speed  $70rad/s$ . When applying 50% external load to the system,  $H_\infty$  controller in Fig.6.6(c) exhibits a less overshoot than that of PI controller, and can converge to original command speed faster than the conventional PI controller as shown in Fig.6.6(a) ( $1.2s$  for  $H_\infty$  and  $2s$  for PI). However, for  $H_\infty$  controller speed undershoot occurs when load is released but it can stabilize almost at the same time as the PI controller ( $4.75s$  for  $H_\infty$  and  $5s$  for PI). When step change in load is applied to the nonlinear PCHD controlled IPMSM, the speed response in Fig.6.6(e) shows the least oscillation than any other controllers developed in this thesis. The shortcoming is that the PCHD controller needs more time in speed recovering after external load is removed.

Fig.6.7 demonstrates the three phase current responses while the motor was running at  $70rad/s$  and 25% rated load. The phase currents validate the balanced operation of the drive system for both nonlinear and PCHD controllers.

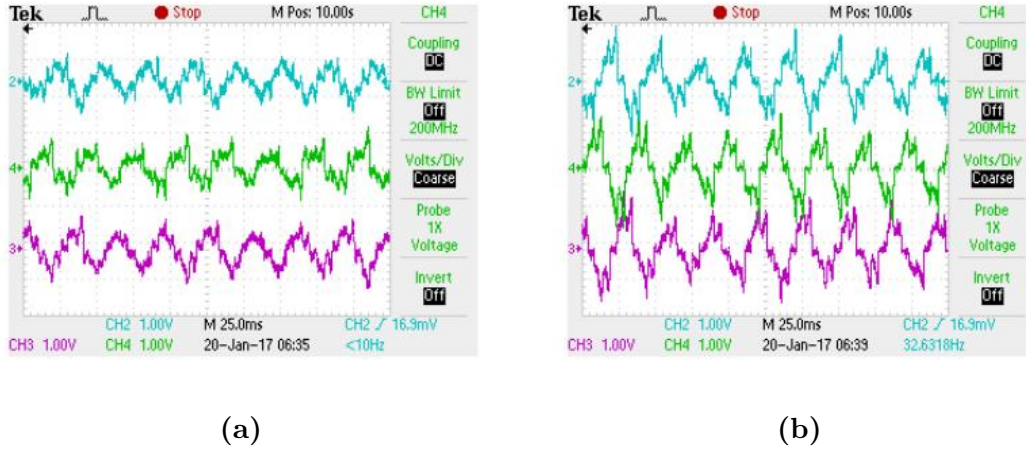


**Figure 6.7:** Experimental performance for balanced three phase currents: (a)  $H_\infty$  controller (b) nonlinear PCHD controller

### 6.3 Conclusion

Proposed  $H_\infty$  and nonlinear PCHD controllers have been tested in a real-time environment for a laboratory 5hp IPMSM to validate the performance in simulation. Two types of step changes have been applied in the chapter, demonstrating the dynamic performance of two controllers. Load change tests have shown controllers' ability to reject torque disturbances. Performance has also been compared with conventional tuned PI controller. As the most commonly used control technique, proposed  $H_\infty$  and nonlinear PCHD controllers show some advantages such as smoother and quicker convergence as compared to the PI controller. The nonlinear PCHD controller exhibited the best performance as compared to both  $H_\infty$  and PI controller.

# Chapter 7

## Conclusion

Based on mathematical analysis, simulation results and a series of real-time experimental tests, it is concluded that the IPMSM is suitable for variable speed and load applications with the developed control algorithms.

### 7.1 Achievements

Mathematical model of IPMSM was derived in the synchronously rotating reference frame at the beginning of this thesis by utilizing two set of coordinate transformations (Park's and Clark's). Park-Clark transformation successfully decoupled torque and flux, making torque control and flux control individually. The model of motor was expressed in state space form for the following controllers design, simulation and real-time experiment.

Two control techniques such as  $H_\infty$  and nonlinear PCHD controllers have been developed in this thesis. Both controller were designed based on the mathematical model of the motor. This class of controller requires online (PI&PCHD) or offline ( $H_\infty$ ) parameters tuning to achieve optimal performance. The basis of the

$H_\infty$  controller is developed under frequency domain and the proof of stability is demonstrated with small gain theorem. Different from the theory of  $H_\infty$ , nonlinear PCHD controller was developed with Hamilton functions, which is an alternative expression of Lyapunov functions. Load estimation is achieved through torque observer, ensuring robust operation in complex operating environment.

Proposed controllers have been simulated using MATLAB/Simulink software. Comparison has been made with conventional PI controller at different operating conditions. Real-time experiment has been achieved with DS1104 embedded board for to a Yaskawa 5hp prototype IPMSM. Comparative results of the proposed controllers with conventional tuned PI controller indicate some of performances have been significantly improved. The nonlinear PCHD demonstrated the least performance in terms of speed setting time and steady-state error as compared to both  $H_\infty$  and PI controllers.

## 7.2 Future scope of the work

As it is shown in the real-time results, the following observations and suggestions have been made for future work.

- Overshoot and undershoot problem in  $H_\infty$  controller can be reduced by using advanced Particle Swarm Optimization (PSO) instead of offline trial and error method in selection of weight functions.
- Adaptive law should be included in nonlinear PCHD controller to reduce the load impact to the speed.
- Implementation of a torque sensor can get more accurate and faster load information instead of mathematical estimation such as torque observer or adaptive law.

# Bibliography

- [1] Xiangjiaba hydropower plant, china. [Online]. Available: <http://www.power-technology.com/projects/xiangjiaba-hydropower-plant/>
- [2] K. Hasse, “Zum dynamischen verhalten der asynchronmaschine bei betrieb mit variabler ständerfrequenz und ständerspannung,” *ETZ-A*, vol. 89, pp. 387–391, 1968.
- [3] F. Blaschke, “Das prinzip der feldorientierung, die grundlage für die transvektor-regelung von drehfeldmaschinen,” *Siemens-Zeitschrift*, vol. 45, no. 10, pp. 757–760, 1971.
- [4] H. A. Malki, D. Misir, D. Feigenspan, and G. Chen, “Fuzzy pid control of a flexible-joint robot arm with uncertainties from time-varying loads,” *IEEE Transactions on Control Systems Technology*, vol. 5, no. 3, pp. 371–378, 1997.
- [5] R. Ketata, D. De Geest, and A. Titli, “Fuzzy controller: design, evaluation, parallel and hierarchial combination with a pid controller,” *Fuzzy sets and systems*, vol. 71, no. 1, pp. 113–129, 1995.
- [6] X. Dai, G. Liu, H. Zhang, and X. Zhang, “Neural network inverse control of variable frequency speed-regulating system in v/f mode,” pp. 6–pp, 2005.

- [7] A. Changuel, A. Jerraya, and R. Rolland, "Design of an adaptive motors controller based on fuzzy logic using behavioral synthesis," in *Proceedings of the conference on European design automation*. IEEE Computer Society Press, 1996, pp. 48–52.
- [8] C. Attaianese, A. Damiano, G. Gatto, I. Marongiu, and A. Perfetto, "Induction motor drive parameters identification," *IEEE Transactions on power electronics*, vol. 13, no. 6, pp. 1112–1122, 1998.
- [9] C. Schauder, "Adaptive speed identification for vector control of induction motors without rotational transducers," *IEEE Transactions on Industry Applications*, vol. 28, no. 5, pp. 1054–1061, 1992.
- [10] L. Liu, X. He, J. Xiao, and H. Weiss, "Model reference adaptive control of asynchronous synchronous motor based on neural network on-line identification," in *Power Electronics and Motion Control Conference, 2006. EPE-PEMC 2006. 12th International*. IEEE, 2006, pp. 961–966.
- [11] K. Ohnishi, Y. Ueda, and K. Miyachi, "Model reference adaptive system against rotor resistance variation in induction motor drive," *IEEE Transactions on Industrial Electronics*, no. 3, pp. 217–223, 1986.
- [12] Y. D. Landau, "Adaptive control: The model reference approach," *IEEE Transactions on Systems, Man, and Cybernetics*, no. 1, pp. 169–170, 1984.
- [13] R. Freeman and P. V. Kokotovic, *Robust nonlinear control design: state-space and Lyapunov techniques*. Springer Science & Business Media, 2008.
- [14] I. Kanellakopoulos, P. V. Kokotovic, and A. S. Morse, "Systematic design of adaptive controllers for feedback linearizable systems," *IEEE Transactions on Automatic control*, vol. 36, no. 11, pp. 1241–1253, 1991.

- [15] M. Ouassaid, M. Cherkaoui, A. Nejmi, and M. Maaroufi, “Nonlinear torque control for pmsm: A lyapunov technique approach,” *World Academy of Science, Engineering and Technology*, pp. 118–121, 2005.
- [16] J. Zhou and Y. Wang, “Real-time nonlinear adaptive backstepping speed control for a pm synchronous motor,” *Control Engineering Practice*, vol. 13, no. 10, pp. 1259–1269, 2005.
- [17] V. Utkin, J. Guldner, and J. Shi, *Sliding mode control in electro-mechanical systems*. CRC press, 2009, vol. 34.
- [18] V. Utkin, “Sliding modes in control and optimization, ser. communications and control engineering series,” 1992.
- [19] H.-P. Jia, D. Sun, and Y.-k. He, “The pmsm dtc based on variable structure sliding mode,” in *Zhongguo Dianji Gongcheng Xuebao(Proceedings of the Chinese Society of Electrical Engineering)*, vol. 26, no. 20, 2006, pp. 134–138.
- [20] L. Y. Z. Guangzhou, “Servo with sliding mode variable structure fuzzy control [j],” *Electric Drive*, vol. 1, p. 006, 2004.
- [21] G. Zames, “Feedback and optimal sensitivity: Model reference transformations, multiplicative seminorms, and approximate inverses,” *IEEE Transactions on automatic control*, vol. 26, no. 2, pp. 301–320, 1981.
- [22] J. Doyle *et al.*, “Analysis of feedback systems with structured uncertainties,” in *IEE proceedings*, vol. 129, no. 6, 1982, pp. 242–250.
- [23] B. Francis and G. Zames, “On h-optimal sensitivity theory for siso feedback systems,” *IEEE Transactions on Automatic Control*, vol. 29, no. 1, pp. 9–16, 1984.

- [24] J. C. Doyle, K. Glover, P. P. Khargonekar, and B. A. Francis, "State-space solutions to standard  $h_2$  and  $h_\infty$  control problems," *IEEE Transactions on Automatic control*, vol. 34, no. 8, pp. 831–847, 1989.
- [25] W. M. Haddad and D. S. Bernstein, "Combined  $l_2/h_\infty$  model reduction," *International Journal of Control*, vol. 49, no. 5, pp. 1523–1535, 1989.
- [26] D. McFarlane and K. Glover, "A loop-shaping design procedure using  $h_\infty$  synthesis," *IEEE transactions on automatic control*, vol. 37, no. 6, pp. 759–769, 1992.
- [27] Y.-H. Chang, T.-H. Liu, and D.-F. Chen, "Design and implementation of a robust controller for a micro permanent magnet synchronous speed control systems," in *Innovative Computing, Information and Control, 2007. ICICIC'07. Second International Conference on*. IEEE, 2007, pp. 99–99.
- [28] G. Wu and X. Xiao, "Robust speed controller for a pmsm drive," in *Power Electronics and Motion Control Conference, 2009. IPEMC'09. IEEE 6th International*. IEEE, 2009, pp. 396–400.
- [29] A. Van der Schaft, *L2-gain and passivity techniques in nonlinear control*. Springer Science & Business Media, 2012.
- [30] R. Ortega, A. J. van der Schaft, and B. M. Maschke, "Stabilization of port-controlled hamiltonian systems via energy balancing," in *Stability And Stabilization Of Nonlinear Systems*. Springer, 1999, pp. 239–260.
- [31] B. M. Maschke and A. J. Schaft, "Port controlled hamiltonian representation of distributed parameter systems," 2000.

- [32] K. Fujimoto and T. Sugie, “Canonical transformation and stabilization of generalized hamiltonian systems,” *Systems & Control Letters*, vol. 42, no. 3, pp. 217–227, 2001.
- [33] W. M. Haddad, S. G. Nersesov, and V. Chellaboina, “Energy-based control for hybrid port-controlled hamiltonian systems,” *Automatica*, vol. 39, no. 8, pp. 1425–1435, 2003.
- [34] R. Ortega, J. A. L. Perez, P. J. Nicklasson, and H. Sira-Ramirez, *Passivity-based control of Euler-Lagrange systems: mechanical, electrical and electromechanical applications*. Springer Science & Business Media, 2013.
- [35] M. Takegaki and S. Arimoto, “A new feedback method for dynamic control of manipulators,” *Journal of Dynamic Systems, Measurement, and Control*, vol. 103, no. 2, pp. 119–125, 1981.
- [36] S. Ge, T. Lee, and G. Zhu, “Energy-based robust controller design for multi-link flexible robots,” *Mechatronics*, vol. 6, no. 7, pp. 779–798, 1996.
- [37] R. Ortega, I. Mareels, A. van der Schaft, and B. Maschke, “Energy shaping revisited,” in *Control Applications, 2000. Proceedings of the 2000 IEEE International Conference on*. IEEE, 2000, pp. 121–126.
- [38] R. Ortega, M. Galaz-Larios, A. S. Bazanella, and A. Stankovic, “Excitation control of synchronous generators via total energy-shaping,” in *American Control Conference, 2001. Proceedings of the 2001*, vol. 2. IEEE, 2001, pp. 817–822.
- [39] R. Ortega, M. W. Spong, F. Gómez-Estern, and G. Blankenstein, “Stabilization of a class of underactuated mechanical systems via interconnection and

- damping assignment,” *IEEE transactions on automatic control*, vol. 47, no. 8, pp. 1218–1233, 2002.
- [40] G. Biros and O. Ghattas, “Parallel lagrange–newton–krylov–schur methods for pde-constrained optimization. part ii: The lagrange–newton solver and its application to optimal control of steady viscous flows,” *SIAM Journal on Scientific Computing*, vol. 27, no. 2, pp. 714–739, 2005.
- [41] A. M. Bloch, N. E. Leonard, and J. E. Marsden, “Controlled lagrangians and the stabilization of mechanical systems. i. the first matching theorem,” *IEEE Transactions on automatic control*, vol. 45, no. 12, pp. 2253–2270, 2000.
- [42] A. M. Bloch, D. E. Chang, N. E. Leonard, and J. E. Marsden, “Controlled lagrangians and the stabilization of mechanical systems. ii. potential shaping,” *IEEE Transactions on Automatic Control*, vol. 46, no. 10, pp. 1556–1571, 2001.
- [43] R. Ortega, A. Van Der Schaft, B. Maschke, and G. Escobar, “Interconnection and damping assignment passivity-based control of port-controlled hamiltonian systems,” *Automatica*, vol. 38, no. 4, pp. 585–596, 2002.
- [44] F. Gómez-Estern and A. J. Van der Schaft, “Physical damping in ida-pbc controlled underactuated mechanical systems,” *European Journal of Control*, vol. 10, no. 5, pp. 451–468, 2004.
- [45] V. Petrovic, R. Ortega, and A. M. Stankovic, “Interconnection and damping assignment approach to control of pm synchronous motors,” *IEEE Transactions on Control Systems Technology*, vol. 9, no. 6, pp. 811–820, 2001.

- [46] C. Batlle, A. Doria-Cerezo, and E. Fossas, “Ida-pbc controller for a bidirectional power flow full-bridge rectifier,” in *Proceedings of the 44th IEEE Conference on Decision and Control*. IEEE, 2005, pp. 422–426.
- [47] S. Nair and N. E. Leonard, “A normal form for energy shaping: application to the furuta pendulum,” in *Decision and Control, 2002, Proceedings of the 41st IEEE Conference on*, vol. 1. IEEE, 2002, pp. 516–521.
- [48] A. Sanz and V. Etxebarria, “Experimental control of a single-link flexible robot arm using energy shaping,” *International journal of systems science*, vol. 38, no. 1, pp. 61–71, 2007.
- [49] C. Batlle Arnau, A. Dòria Cerezo, E. Fossas Colet, and R. Ortega, “Energy-based modelling and control of a multi-domain energy storage and management system,” 2006.
- [50] J.-E. Slotine and M. Di Benedetto, “Hamiltonian adaptive control of spacecraft,” *IEEE Transactions on Automatic Control*, vol. 35, no. 7, pp. 848–852, 1990.
- [51] R. Ortega, A. J. Van Der Schaft, I. Mareels, and B. Maschke, “Putting energy back in control,” *IEEE Control Systems*, vol. 21, no. 2, pp. 18–33, 2001.
- [52] J.-H. Kim, K.-C. Kim, and E. K. Chong, “Fuzzy precompensated pid controllers,” *IEEE Transactions on control systems technology*, vol. 2, no. 4, pp. 406–411, 1994.
- [53] S. Chiu, “Using fuzzy logic in control applications: beyond fuzzy pid control,” *IEEE control systems*, vol. 18, no. 5, pp. 100–104, 1998.

- [54] H. B. Kazemian, “Comparative study of a learning fuzzy pid controller and a self-tuning controller,” *ISA transactions*, vol. 40, no. 3, pp. 245–253, 2001.
- [55] T. T. Shannon and G. G. Lendaris, “Adaptive critic based design of a fuzzy motor speed controller,” in *Intelligent Control, 2001.(ISIC’01). Proceedings of the 2001 IEEE International Symposium on.* IEEE, 2001, pp. 359–363.
- [56] E. Cerruto, A. Consoli, A. Raciti, and A. Testa, “Fuzzy adaptive vector control of induction motor drives,” *IEEE Transactions on Power Electronics*, vol. 12, no. 6, pp. 1028–1040, 1997.
- [57] W. S. McCulloch and W. Pitts, “A logical calculus of the ideas immanent in nervous activity,” *The bulletin of mathematical biophysics*, vol. 5, no. 4, pp. 115–133, 1943.
- [58] F.-J. Lin, R.-J. Wai, and C.-C. Lee, “Fuzzy neural network position controller for ultrasonic motor drive using push-pull dc-dc converter,” *IEE Proceedings-Control Theory and Applications*, vol. 146, no. 1, pp. 99–107, 1999.
- [59] M. Rahman and M. Hoque, “Online adaptive artificial neural network based vector control of permanent magnet synchronous motors,” *IEEE Power Engineering Review*, vol. 17, no. 9, pp. 28–28, 1997.
- [60] W. SUN and Y.-n. WANG, “Ac servo system based on fuzzy gauss function neural network control [j],” *ELECTRIC MACHINES AND CONTROL*, vol. 2, p. 005, 1999.
- [61] S.-H. Kim, T.-S. Park, J.-Y. Yoo, and G.-T. Park, “Speed-sensorless vector control of an induction motor using neural network speed estimation,” *IEEE Transactions on Industrial Electronics*, vol. 48, no. 3, pp. 609–614, 2001.

- [62] W. Dazhi, G. Shusheng, and W. Kenan, “A neural-network-base adaptive estimator for speed-sensorless control of induction motor,” in *Intelligent Control and Automation, 2002. Proceedings of the 4th World Congress on*, vol. 4. IEEE, 2002, pp. 2812–2816.
- [63] S. Boyd and C. A. Desoer, “Subharmonic functions and performance bounds on linear time-invariant feedback systems,” *IMA Journal of Mathematical control and Information*, vol. 2, no. 2, pp. 153–170, 1985.
- [64] J. C. Willems, “Dissipative dynamical systems part i: General theory,” *Archive for rational mechanics and analysis*, vol. 45, no. 5, pp. 321–351, 1972.
- [65] H. Goldstein, *Classical mechanics*. Pearson Education India, 1965.
- [66] V. I. Arnol’d, *Mathematical methods of classical mechanics*. Springer Science & Business Media, 2013, vol. 60.

# Appendix A

## IPMSM Parameters

**Table A.1:** IPMSM Parameters

Rated power	$P_{rated}$	3.7 kW
Rated Speed	$\omega_{rated}$	183 rad/s
Rated voltage	$V_{rated}$	183 V
Rated frequency	$f_{rated}$	87.5 Hz
Rated current	$I_{rated}$	14.2 A
Pole pairs	$N_p$	3
d-axis inductance	$L_d$	5.06 mH
q-axis inductance	$L_q$	6.42 mH
Stator resistance	$R_s$	0.424 $\Omega$
Inertia constant	$J$	0.0133 Kg $\cdot$ m <sup>2</sup>
Damping coefficient	$B_m$	0.001 Nm/rad/s
Magnetic flux constant	$\phi_m$	0.2449 V/rad/s

# Appendix B

## Simulation Code and Schematic

The details of the subsystem blocks and controller tuning code for simulation and real-time propose is shown in this section. Section B.1 shows the tuning code for the proposed  $H_\infty$  controller. Simulation sub-blocks shown in section B.2 as references for Fig.5.1. Real-time schematic for both  $H_\infty$  and nonlinear PCHD controller is demonstrated in section B.3.

### B.1 $H_\infty$ controller offline tuning code

```
For both Simulation and Real-time
%IPMSM Parameters
Rs    = 0.242;
Ld    = 0.00506;
Lq    = 0.00642;
PHIm  = 0.2449;
Np    = 3;
J     = 0.0133;
Bm    = 0.001;

%PI controller for q-axis current
kp    = 4.5;
ki    = 0.9;
```

```

%Transfer Functions
s = tf('s');
Gi = Kr/(Tr*s+1);
Ga = 1/(Lq*s+Rs);
Gm = 1/(J*s+Bm);
Kt = 3*Np*PHIm/2;
Kf = Np*PHIm;
P = Ga*Gi*Gm*Kt/(Ga*Gi+Ga*Gm*Kt*Kf+1);

%Weight Functions (following functions are used for
simulation)
W1 = (5*s+100)/(10*s+0.1);
W2 = 0.008;
W3 = (3*s+5)/(0.1*s+1000);

Ga = augw(P,W1,W2,W3);
[Ccss,CL,GAM,INFO] = hinfsyn (Ga);

[Gcss_num, Gcss_den] = ss2tf (Ccss.a,Ccss.b,Ccss.c,Ccss.
d)
Cctf = tf (Gcss_num, Gcss_den);
zpk(Cctf);
Cdss = (c2d(Ccss,1e-4));

```

## B.2 Simulation and Real-time Schematic

### B.2.1 Simulation Schematic

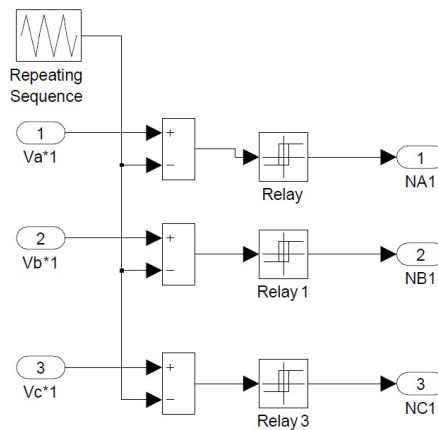


Figure B.1: Sybsystem of PWM generation

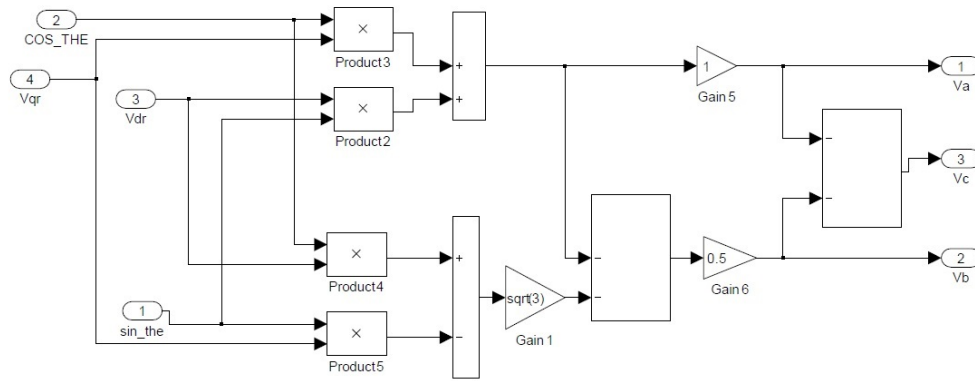


Figure B.2: Subsystem of d-q axis voltage to a-b-c axis voltage

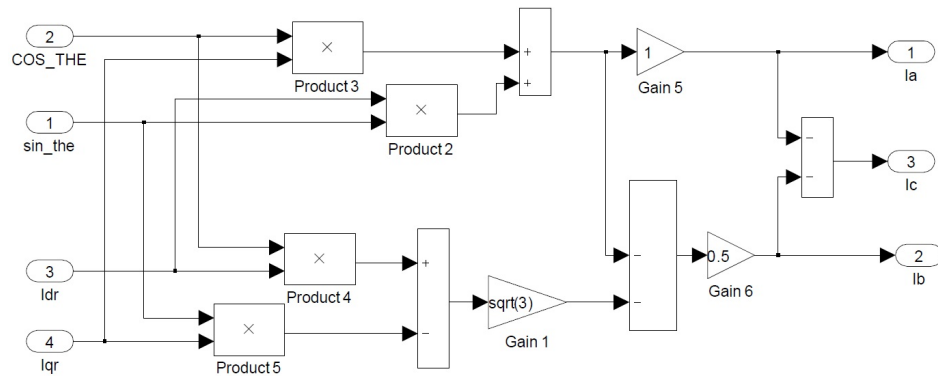


Figure B.3: Subsystem of d-q axis current to a-b-c axis current

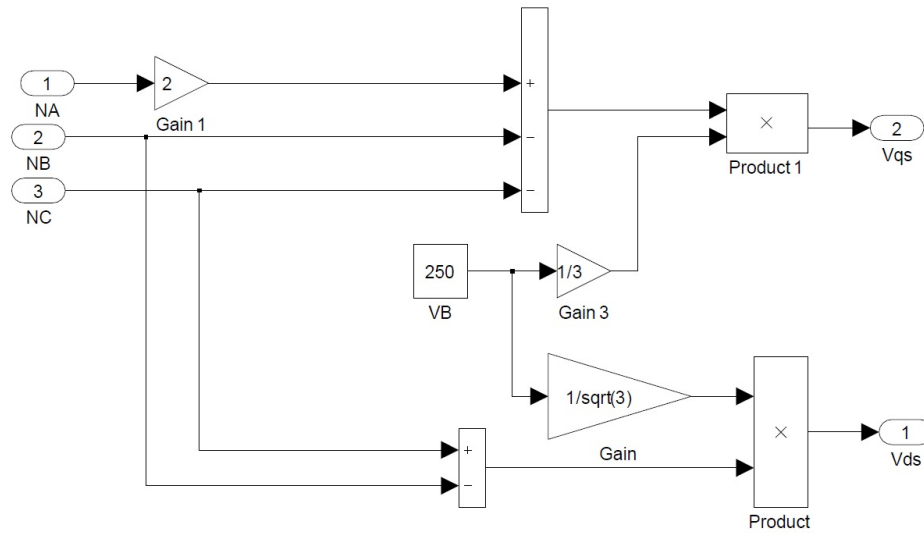


Figure B.4: Subsystem of inverter

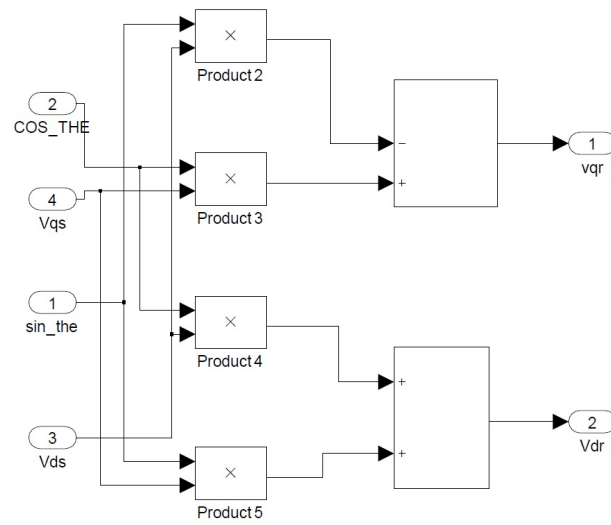


Figure B.5: Subsystem of  $\alpha$ - $\beta$  axis voltage to d-q axis voltage

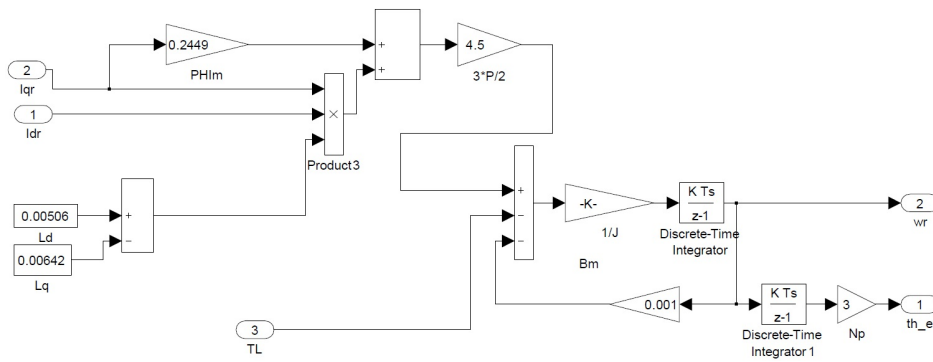


Figure B.6: Subsystem of rotor speed

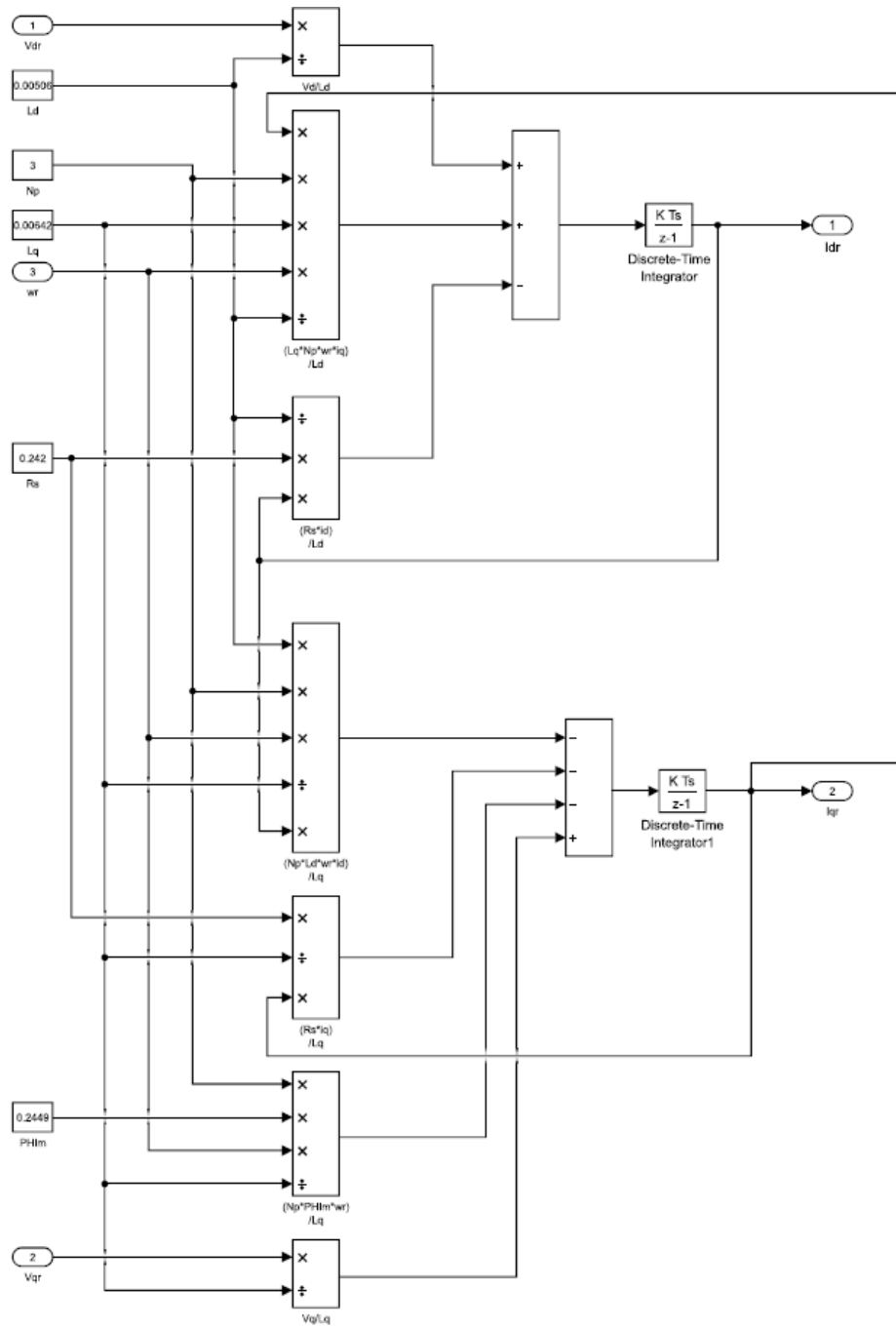


Figure B.7: Subsystem of rotor current



## B.3 Real-time Schematic

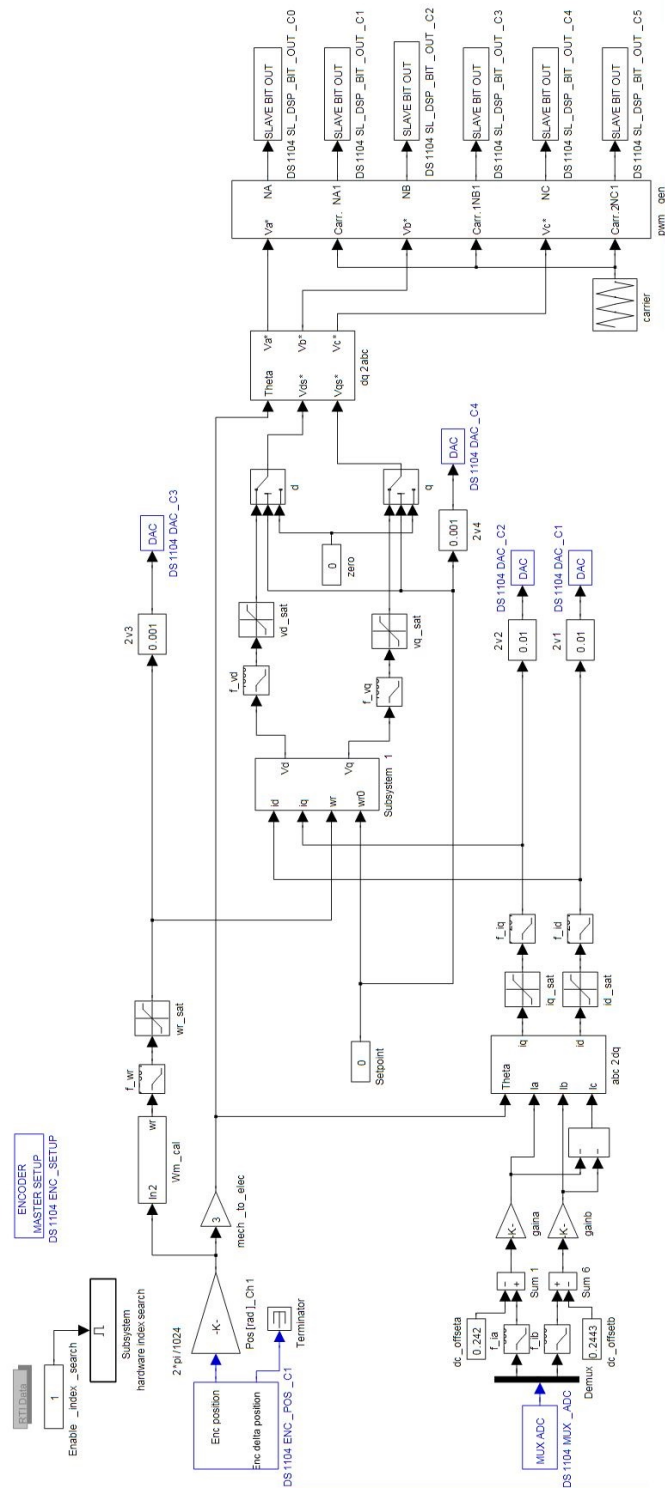


Figure B.9: Real-time Simulink Blocks.